Epitaxially Driven Assembly of Crystalline Molecular Films on Ordered Substrates

Julie A. Last, Andrew C. Hillier,† Daniel E. Hooks, Jeffrey B. Maxson, and Michael D. Ward*

Department of Chemical Engineering and Materials Science, University of Minnesota, Amundson Hall, 421 Washington Avenue SE, Minneapolis, Minnesota 55455

Received August 20, 1997. Revised Manuscript Received October 27, 1997⊗

Crystalline, molecularly thick organic films mimicking layer motifs observed in bulk crystals of conducting $(ET)_2X$ charge-transfer salts (ET = bis(ethylenedithiolo)tetrathiafulvalene, X = I_3, ReO_4) form on highly oriented pyrolytic graphite (HOPG) electrodes upon electrochemical oxidation of ET in electrolytes containing I_3^- or ReO_4^- anions. The assembly of these molecular overlayers can be observed directly by in situ atomic force microscopy (AFM), and their structures can be deduced from lattice images obtained by AFM under growth conditions. AFM data reveal two different $(ET)_2I_3$ overlayers that are distinguished by the orientation of the ET molecules. One of these overlayers (type I) exhibits lattice structure and thickness corresponding to the (001) layer of bulk β-$(ET)_2I_3$, while the other (type II) exhibits structural characteristics consistent with a slightly reconstructed version of the (110) layer in crystalline β-$(ET)_2I_3$. In contrast, $(ET)_2ReO_4$ overlayers exhibit only the type II orientation, which resembles the (011) layer of bulk $(ET)_2ReO_4$. Comparison of the overlayer azimuthal orientation with respect to the underlying HOPG substrate, determined directly by AFM, reveals that each overlayer forms by coincident epitaxy in which strict commensurism is achieved only at the vertexes of a supercell comprising an array of primitive unit cells. The observed azimuthal orientations are in agreement with values predicted by either potential energy calculations or an analytical model of the overlayer−substrate interface. Strong two-dimensional intralayer interactions in the type I (001) β-$(ET)_2I_3$ overlayer and a coincident lattice match favor the formation of a crystalline layer in which the structure mimicks the bulk layer structure. However, the type II overlayers are oriented such that only one strong intralayer bonding vector remains, facilitating slight reconstructions from the bulk layer structures so that coincidence can be achieved. Calculations of overlayer−substrate and overlayer energies and elastic constants indicate that although coincident epitaxy between the (001) $(ET)_2ReO_4$ overlayer and HOPG is possible, the accumulation of interfacial stresses from noncommensurate overlayer sites within its large supercell prevents its formation. These observations, when combined with analysis of the intralayer and overlayer−substrate elastic constants, indicate that the overlayer structure and its orientation with respect to the substrate are governed by the epitaxial relationship between the substrate and large ordered arrays of molecules, reflecting a delicate balance of intralayer and overlayer−substrate energetics. The design strategy based on bulk crystallographic layers and the overlayer−substrate epitaxy represents a "crystal engineering" approach to the fabrication of molecular thin films.

Introduction

Interest in molecular materials for electronic devices, sensors, displays, and logic elements[1] stems primarily from the potential for systematic manipulation of the bulk optical and electronic properties by alteration of the molecular structure of the constituents. The combination of molecular design and crystal engineering strategies[2] has led to the synthesis of crystalline materials with desirable properties such as conductivity and superconductivity,[3] ferromagnetism,[4] and nonlinear optical behavior.[5] Although most of these efforts have been directed toward the synthesis of bulk materials, crystalline molecular films immobilized on rigid sub-

† Current address: Department of Chemical Engineering, University of Virginia, Charlottesville, VA 22903-2442.

* To whom correspondence should be addressed.

⊗ Abstract published in *Advance ACS Abstracts,* December 15, 1997.

(1) (a) Aviram, A.; Ratner, M. *Chem. Phys. Lett.* **1972**, *29*, 277. (b) Carter, F. L., Ed. *Molecular Electronic Devices*; Marcel Dekker: New York, 1982. (c) Ashwell, G. J., Ed. *Molecular Electronics*; John Wiley & Sons: New York, 1992.

(2) (a) Desiraju, G. *Crystal Engineering—The Design of Organic Solids*; Elsevier: New York, 1989. (b) Fagan, P. J.; Ward, M. D.; Calabrese, J. C. *J. Am. Chem. Soc.* **1989**, *111*, 1698.

(3) (a) Miller, J. *Extended Linear Chain Compounds*; Plenum Press: New York, 1982−84; Vol. 1−3. (b) Williams, J. M.; Wang, H. H.; Emge, T. J.; Geiser, U.; Beno, M. A.; Leung, C. W.; Carlson, K.d.; Thorn, R. J.; Schultz, A. J. In *Progress in Inorganic Chemistry*; Lippard, S. J., Ed.; John Wiley and Sons: New York, 1987; p 51. (c) Williams, J. M.; Schultz, A. J.; Geiser, U.; Carlson, K. D.; Kini, A. M.; Wang, H. H.; Kwok, W.-K.; Whangbo, M.-H.; Schirber, J. E. *Science* **1991**, *252*, 1501.

(4) Miller, J. S.; Epstein, A. J.; Reiff, W. M. *Science* **1988**, *240*, 40.

(5) Zyss, J.; Tscoucaris, G. *Structure and Properties of Molecular Crystals*; Pierrot, M., Ed; Elsevier: Amsterdam, 1990.

S0897-4756(97)00582-6 CCC: $15.00
Published on Web 01/19/1998

strates may provide new opportunities. Substrates can provide addressibility as well as mechanical stability for these otherwise fragile materials. Light-emitting diodes,[6−9] field effect transistors,[10−15] and devices with photovoltaic properties,[16,17] based on films of molecular crystals have been reported recently. The properties of molecular films will hinge on control of their supramolecular structure, their orientation with respect to the substrate, and the nature and distribution of defects. Elucidating the influence of the substrate on these film characteristics is crucial to the advancement of thin-film technologies that use these materials.

Recent efforts in our laboratory have been aimed toward the design and synthesis of crystalline molecular films on ordered substrates in which the preferred native structure of the primary molecular overlayer, presumed to be at or near its minimum energy configuration, is based on layered motifs existing in the corresponding bulk crystals.[18,19] The tendency of molecules to assemble in the solid state into two-dimensional (2-D) layers with strong intralayer bonding (e.g., through hydrogen-bonding, charge-transfer, or heteroatom−heteroatom interactions) suggests that layered motifs in bulk crystals are ideal design elements for the fabrication of robust heteroepitaxial films on appropriately chosen substrates. Although many molecular films have been grown on amorphous substrates, growth on a crystalline substrate can be influenced by epitaxy between the substrate and a primary overlayer. The influence of epitaxy on the structure and properties of inorganic films has been examined extensively and is well documented.[20] However, fundamental studies directed at elucidating the "soft" interface between molecular overlayers and ordered substrates has been rather limited. Molecular overlayers are unique in that commensurism, in which the overlayer and substrate lattices are in registry so that attractive interatomic potentials are reinforced across the entire overlayer−substrate interface, is unlikely due to the inherently low symmetry and large lattice dimensions of most molecular overlayers. Furthermore, weak noncovalent interactions within the overlayers may make them susceptible to structural changes due to interaction with the substrate;[21,22] in the extreme case an overlayer can expand to a less densely packed form to become commensurate with the substrate. Elucidation and control of overlayer assembly therefore relies on development of guiding principles, similar to crystal engineering principles devised for three-dimensional molecular solids, but in which the role of the substrate is considered. This requires investigation of the overlayer assembly process, structural characterization of the overlayer and overlayer−substrate interface, and analysis of the overlayer and overlayer−substrate energetics.

We describe herein investigations of the assembly of highly crystalline molecular overlayers on ordered substrates by real-time in situ atomic force microscopy (AFM), which enables direct examination of overlayer assembly and determination of the structure of the overlayer and its orientational relationship with the substrate. The overlayers described here, grown on a highly oriented pyrolytic graphite (HOPG) electrode, are based on specific crystal planes in the conductive charge-transfer salts $(ET)_2X$ (ET = bis(ethylenedithiolo)-tetrathiafulvalene; X = I_3, ReO_4).[23,24] These salts were chosen for three principal reasons: (i) the bulk crystals were intrinsically 2-D because of strong $\pi-\pi$ overlap between the molecules along one dimension and strong dispersive interactions between polarizable heteroatoms along a second dimension, which should favor overlayers that are structurally robust and amenable to study, (ii) the ability to grow the films electrochemically enabled regulation of nucleation and growth that was not achievable with redox-inert systems, and (iii) the growth of these films occurs under ambient conditions so that their assembly can be examined directly with AFM. The assembly of these molecular overlayers is governed by *coincident* epitaxy, in which strict "point-on-point" commensurism between a densely packed overlayer and the HOPG substrate is achieved only at the vertexes of a supercell comprising several primitive unit cell of the overlayer. Overlayer sites within this supercell are noncommensurate, although they can be described as having less favorable "point-on-line" coincidence in which the overlayer molecules sit on a specific substrate lattice vector.[25] These studies illustrate that overlayer structure and orientation with respect to the substrate are governed by interactions between the substrate and large ordered arrays of molecules rather than individual substrate−molecule interactions, the overlayer configuration reflecting a delicate balance of these interactions and intermolecular interactions within the overlayer. The assembly of these overlayers, which are the precursor nuclei for bulk crystals, provides insight into crystal nucleation, growth, polymorphism, and morphology.

Experimental Section

Materials. Solutions of bis(ethylenedithiolo)tetrathiafulvalene (ET, Strem Chemicals, Newburyport, MA, or Aldrich,

(6) Strukelj, M.; Jordan, R. H.; Dodabalapur, A. *J. Am. Chem. Soc.* **1996**, *118*, 1213.
(7) Kido, J.; Kimura, M.; Nagaim, K. *Science* **1995**, *67*, 1332.
(8) Tang, C. W.; Van Slyke, S. A.; Chen, C. H. *J. Appl. Phys.* **1989**, *65*, 3610.
(9) Tang, C. W.; Van Slyke, S. A. *Appl. Phys. Lett.* **1987**, *51*, 913.
(10) Horowitz, G.; Kouki, F.; Spearman, P.; Fichou, D.; Nogues, C.; Pan, X.; Garnier, F. *Adv. Mater.* **1996**, *8*, 242.
(11) Greenham, N. C.; Moratti, S. C.; Bradley, D. D. C.; Friend, R. H.; Holmes, A. B. *Nature* **1993**, *44*, 201.
(12) Hiramato, M.; Fujiwara, H.; Yokoyama, M. *Appl. Phys. Lett.* **1991**, *58*, 1062.
(13) Hiramato, M.; Fujiwara, H.; Yokoyama, M. *J. Appl. Phys.* **1992**, *72*, 3781.
(14) Haddon, R. C.; Perel, A. S.; Morris, R. C.; Palstra, T. T. M.; Hebard, A. F.; Fleming, R. M. *Appl. Phys. Lett.* **1995**, *67*, 121.
(15) Brown, A. R.; Deleeuw, D. M.; Lous, E. J.; Havinga, E. E. *Synth. Met.* **1994**, *66*, 257.
(16) Tang, C. W. *Appl. Phys. Lett.* **1986**, *48*, 183.
(17) Liu, C.-Y.; Lynch, V.; Bard, A. *J. Chem. Mater.* **1997**, *9*, 943.
(18) Scaringe, R. P. In *Electron Crystallography of Organic Molecules*; Fryer, J. R.; Dorset, D. L., Eds.; Kluwer: Boston, **1991**; p 85.
(19) Perlstein, J. *J. Am. Chem. Soc.* **1994**, *116*, 11420.
(20) *Epitaxial Growth*; Matthews, J., Ed.; Academic Press: New York, 1975.
(21) Hossick-Schott, J.; Ward, M. D. *J. Am. Chem. Soc.* **1994**, *116*, 6806.
(22) Hossick-Schott, J.; Yip, C. M.; Ward, M. D. *Langmuir* **1995**, *11*, 177.
(23) Hillier, A. C.; Maxson, J. B.; Ward, M. D. *Chem. Mater.* **1994**, *6*, 2222.
(24) Hillier, A. C.; Hossick-Schott, J.; Ward, M. D. *Adv. Mater.* **1995**, *7*, 409.
(25) Hillier, A. C.; Ward, M. D. *Phys. Rev. B* **1996**, *54*, 14037.

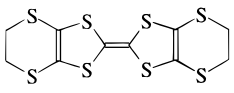

ET

Milwaukee, WI) were prepared in HPLC grade (EM Science, Gibbstown, NJ) or distilled acetonitrile. n-$Bu_4N^+I_3^-$ was prepared by a previously reported procedure[26] in which I_2 was added to a boiling solution of chloroform or water containing excess n-$Bu_4N^+I^-$ (Aldrich, Milwaukee, WI). The resulting black precipitate was recrystallized twice from methanol to provide dark, lustrous crystals of n-$Bu_4N^+I_3^-$. Electrolytes n-$Bu_4N^+ClO_4^-$ and n-$Bu_4N^+ReO_4^-$ were obtained commercially (Aldrich, Milwaukee, WI) and were recrystallized from ethanol.

Methods. Electrochemical synthesis and in situ atomic force microscopy (AFM) of $(ET)_2I_3$ and $(ET)_2ReO_4$ overlayers were performed in a commercially available fluid cell (Digital Instruments, Santa Barbara, CA) adapted for electrochemical growth, as described previously.[27,28] A three-electrode design was employed for electrochemical measurements with a highly oriented pyrolytic graphite (HOPG) substrate (Union Carbide) serving as the working electrode, with Pt counter and reference electrodes placed in the outlet of the fluid cell. All electrode potentials are reported with respect to a Ag/AgCl reference. The HOPG substrate electrode was cleaved to expose a fresh surface prior to use. Overlayers of $(ET)_2X$ were grown by electrochemical oxidation of ET in acetonitrile containing ET and I_3^- or ReO_4^- under conditions similar to those reported for the electrosynthesis of bulk crystals.[23,24,29]

AFM experiments were performed with a Nanoscope III Multimode scanning probe microscope (Digital Instruments, Santa Barbara, CA). AFM probes (Nanoprobe, Park Scientific, Sunnyvale, CA or Digital Instruments, Santa Barbara, CA) consisted of triangular silicon nitride cantilevers (force constant = 0.06 N m^{-1}) with integrated pyramidal tips. The AFM was equipped with a scan head having a maximum scan range of 15 μm by 15 μm. AFM images were acquired in the contact mode under nominally constant force conditions. The tip−sample force was minimized before imaging by reducing the set point to a value just below tip disengagement. The azimuthal orientation of the $(ET)_2X$ overlayers with respect to the HOPG substrate was determined by imaging an exposed region of the substrate immediately before or after imaging of the overlayer, or by imaging the substrate lattice underneath the overlayer after removing the overlayer mechanically by increasing the force exerted by the AFM tip.

Determination of the mode of epitaxy and optimum overlayer orientation was accomplished using EpiCalc, which runs in the Windows v. 3.1 or Windows 95 environment on a Pentium personal computer. EpiCalc, which uses an analytical function devised in our laboratory,[25] requires as input the 2-D lattice parameters for the substrate and overlayer. The output includes the dimensionless potential energy, V/V_0, and the transformation matrix elements, which describe the overlayer orientation in terms of the substrate lattice vectors, as a function of overlayer rotation angle over a user-defined range at a user-defined increment. The value of V/V_0 indicates the degree of commensurism; an incommensurate overlayer returns $V/V_0 = 1$, a coincident overlayer returns $V/V_0 = 0.5$, and a commensurate overlayer returns $V/V_0 = 0$ for a nonhexagonal substrate or $V/V_0 = -0.5$ for a hexagonal substrate. EpiCalc allows the user to specify a range of lattice parameters to search for coincident reconstructed forms of the overlayer, reporting V/V_0 as a function of both overlayer rotation angle and lattice parameters. EpiCalc is available on the World Wide Web at http://www.cems.umn.edu/research/ward.

Potential energy calculations for the overlayer−substrate interfaces were performed on a Hewlett-Packard 710 workstation using a Universal Force Field[30] based on a Lennard-Jones 6−12 potential function. These calculations were integrated with a Fortran code that allowed approach, translation, and rotation of an overlayer−substrate molecular interface. Energy-minimized overlayer structures and intralayer potentials also were calculated using the Cerius molecular modeling program (Molecular Simulations, v 1.6, 2.0) and the Universal Force Field. The Lennard-Jones 6−12 potential function has a high-curvature potential well and an easily determined minimum compared to potential wells associated with Coulombic interactions, which are relatively broad. Consequently, the change in lattice energy resulting from small dimensional changes about the minimum energy structure is more sensitive to the Lennard-Jones 6−12 potential function than to Coulombic or dipole terms. Furthermore, the minimized overlayer structures calculated with only the Lennard-Jones 6−12 potential function were essentially identical with those of the corresponding layers in their bulk crystals. This argues that the Lennard-Jones function can be used to predict overlayer dimensions and elastic constants (see below) for these systems and that the "native" layered motifs in bulk crystals can be used as a guide for overlayer design. These layered motifs can be obtained from crystal structures available in the Cambridge Structural Database (version 2.3.7). In the examples described here, the native structures present in bulk crystals served as the initial structures in energy minimization and intralayer potential calculations. Stress and elastic constants were determined directly from the calculated potentials. The minimum energy overlayer−substrate separation, $E_{min}(z)$, was determined by positioning the origin of the overlayer unit cell (taken as the origin of its crystallographic analog) over the crystallographic origin of the HOPG substrate at the intersection of its principal lattice vectors. Similarly, the elastic constant associated with the stress and strain normal to the overlayer−substrate interface, c_{zz}, was calculated with the overlayer and substrate origins aligned. All elastic constants were calculated with the overlayer at the optimum azimuthal angle, which was determined by either potential energy calculations or with EpiCalc, using a single-overlayer unit cell as a basis. Substrate−overlayer energies for different overlayer sizes were compared after muliplication by a normalization factor equal to the quotient of the number of pairwise interactions between the supercell and the substrate for the overlayer and that for the (001) $(ET)_2ReO_4$ $3\mathbf{b_1} \times 4\mathbf{b_2}$ supercell (93 000 interactions). Structural models were visualized with the Computer Assisted Chemistry (CAChe, Inc.) molecular modeling program.

Results and Discussion

Structure of Molecular Layers in ET Salts. Molecular charge-transfer salts containing ET have been examined extensively because of their conductivity and superconductivity.[3] These salts, like many molecular crystals, typically exhibit layered motifs in which at least one molecular layer can be identified by the presence of strong 2-D interactions within that layer. The presence of strong 2-D intralayer bonding and the corresponding low surface energy of these molecular planes suggest that such layer motifs are optimum candidates for robust crystalline mono- and multilayer films. These layers, which can be identified readily by inspection of the crystal structures of $(ET)_2X$ salts (ET

(26) (a) Bender, K.; Hennig, I.; Schweitzer, D.; Dietz, K; Endres, H.; Keller, H. *Mol. Cryst. Liq. Cryst.* **1984**, *108*, 359. (b) Emge, T. J.; Leung, P.; Beno, M. *Mol. Cryst. Liq. Cryst.* **1986**, *132*, 363.

(27) Hillier, A. C.; Ward, M. D. *Science* **1994**, *263*, 1261.

(28) Carter, P. W.; Hillier, A. C.; Ward, M. D. *J. Am. Chem. Soc.* **1994**, *116*, 944.

(29) (a) Engler, E. M.; Lee, V. Y.; Schumaker, R. R.; Parkin, S. S. P.; Greene, R. L.; Scott, J. C. *Mol. Cryst. Liq. Cryst.* **1984**, *107*, 19. (b) Carneiro, K.; Scott, J. C.; Engler, E. M. *Solid State Commun.* **1984**, *50*, 477. (c) Williams, J. M.; Beno, M. A.; Wang, H. H.; Reed, P. E.; Azevedo, L. J.; Schriber, J. E. *Inorg. Chem.* **1984**, *23*, 1790. (d) Parkin, S. S.; Engler, E. M.; Schumaker, R.; Lagier, R.; Lee, V. Y.; Scott, J. C.; Greene, R. L. *Phys. Rev. Lett.* **1983**, *50*, 270.

(30) Rappe, A. K.; Casewit, C. J.; Colwell, K. S.; Goddard, W. A. III; Skiff, W. M. *J. Am. Chem. Soc.* **1992**, *114*, 10024.

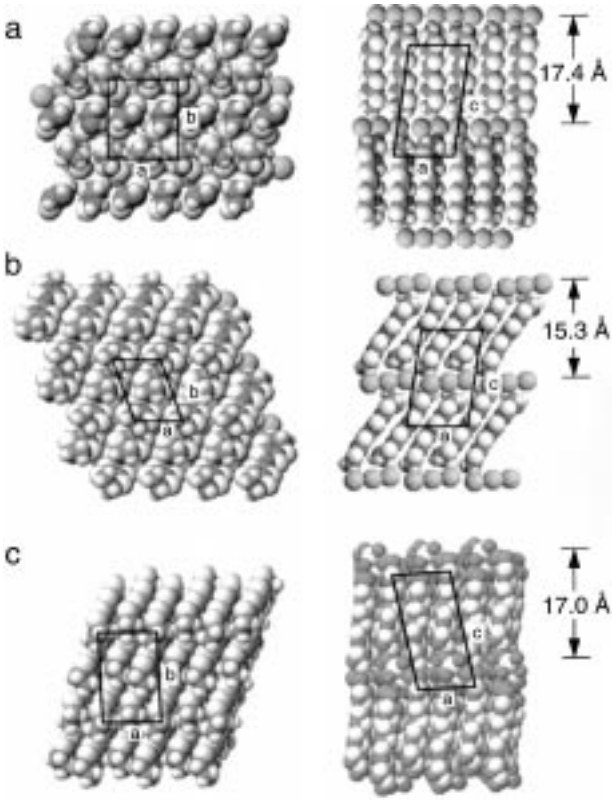

Figure 1. Normal views of the molecular packing in the (001) and (010) planes of (a) α-$(ET)_2I_3$, (b) β-$(ET)_2I_3$, and (c) $(ET)_2ReO_4$ salts. The (001) planes are depicted with the ET layers facing up. The numbers at the right of the (010) views correspond to the (001) layer thicknesses.

= bis(ethylenedithiolo)tetrathiafulvalene; X = I_3, ReO_4), typically contain fractionally charged $ET^{0.5+}$ molecules separated by X^- layers.[31] The $(ET)_2I_3$ and $(ET)_2ReO_4$ salts, which exhibit numerous polymorphs, are illustrative in this respect (Figure 1).

The structure of α-$(ET)_2I_3$ consists of (001) layers containing stacks of ET molecules assembled along [100] by $\pi-\pi$ charge-transfer interactions, with the stacks organized in a herringbone pattern along the [010] direction by S···S van der Waals interactions between molecules in adjacent stacks (Figure 1a). The occurrence of these two strong bonding vectors impart a low surface energy to the (001) plane, consistent with the observation that the (001) face of bulk crystals of α-$(ET)_2I_3$ has the largest area. The structure of β-$(ET)_2I_3$ also consists of (001) layers which contain cations assembled by $\pi-\pi$ charge-transfer interactions along [011] stacks with the stacks assembled by S···S van der Waals interactions along [100] (Figure 1b). Consequently, the (001) plane of β-$(ET)_2I_3$ also has a low surface energy as evidenced by the large (001) faces in bulk crystals of this phase. Inspection of the crystal structures reveals that the (001) layers of α- and β-$(ET)_2I_3$ differ substantially with respect to the layer

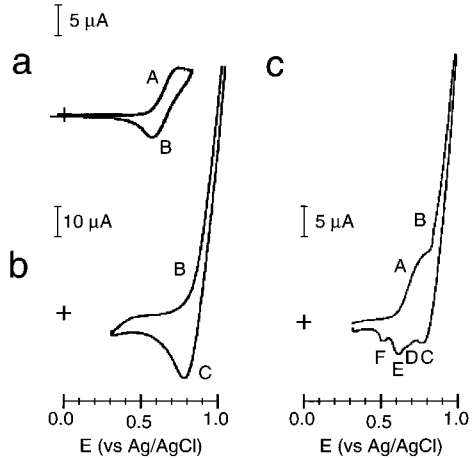

Figure 2. Cyclic voltammetry of ET and *n*-$Bu_4N^+I_3^-$ in CH_3CN at a 9 mm diameter freshly cleaved HOPG electrode: (a) 0.5 mM ET in 0.1 M *n*-$Bu_4N^+ClO_4^-$; (b) 10 mM *n*-$Bu_4N^+I_3^-$ in 0.1 M *n*-$Bu_4N^+ClO_4^-$; (c) 0.5 mM ET and 10 mM *n*-$Bu_4N^+I_3^-$ in 0.1 M *n*-$Bu_4N^+ClO_4^-$.

heights (17.42 and 15.28 Å, respectively), molecular packing patterns, and 2-D lattice parameters.[32]

Similar layer motifs are present in $(ET)_2ReO_4$ and three polymorphs of $(ET)_3(ReO_4)_2$. Lattice parameters have been reported for each of these phases, but structural coordinates have been provided only for the superconducting triclinic phase $(ET)_2ReO_4$.[33] This phase contains alternating (001) layers of ET cations and ReO_4^- anions in which the ET molecules stack by $\pi-\pi$ charge-transfer interactions along [100] (*a*-axis) and the stacks assemble along [010] (*b*-axis) by S···S van der Waals interactions (Figure 1c). Consequently, the (001) plane has the lowest surface energy and the (001) face has the largest area, similar to the α- and β-$(ET)_2I_3$ phases.

Electrochemical Behavior and Electrocrystallization. Previous studies of the electrocrystallization of $(ET)_2I_3$ salts have demonstrated that the choice of electrocrystallization conditions influences the selectivity toward the α and β polymorphs, with the kinetically favored α-phase forming at high overpotentials and the thermodynamically favored β-phase forming at low overpotentials.[34] Furthermore, electrocrystallization on electrochemically etched HOPG favors formation of the α-phase, whereas the β-phase forms on pristine HOPG surfaces.[35] Electrochemical parameters also influence polymorph selectivity during growth of the $ET_x(ReO_4)_y$ salts. Low currents (<1 μA) typically produced the α-3:2 phase, while a mixture of the β-3:2 and 2:1 phases was obtained at intermediate currents (1−3 μA).[29] These observations suggest that the electrode surface and

(31) (a) Williams, J. M.; Ferraro, J. R.; Thorn, R. J.; Carlson, K. D.; Geiser, U.; Wang, H. H.; Kini, A. M.; Whangbo, M. *Organic Superconductors (Including Fullerenes)*; Prentice Hall: Upper Saddle river, NJ, 1992. (b) Carlson, K. D.; Wang, H. H.; Beno, M. A.; Kini, A. M.; Williams, J. M. *Mol. Cryst. Liq. Cryst.* **1990**, *181*, 91. (c) Shibaeva, R. P.; Yagubskii, E. B.; Laukhina, E. E.; Laukhin, V. N. In *The Physics and Chemistry of Organic Superconductors*; Saito, G., Kagoshima, S., Eds.; Springer-Verlag: Berlin, 1990; p 342.

(32) The lattice parameters for α-$(ET)_2I_3$ are a = 9.183 Å, b = 10.804 Å, c = 17.422 Å, α = 96.96°, β = 97.93°, γ = 90.85°.

(33) The crystal structures of three forms of $(ET)_3(ReO_4)_2$ have been reported but structural coordinates were not included.[29] Monoclinic α-$(ET)_3(ReO_4)_2$: a = 8.50 Å, b = 30.57 Å, c = 9.41 Å, β = 89.6°; triclinic β-$(ET)_3(ReO_4)_2$: a = 9.28 Å, b = 16.11 Å, c = 8.37 Å, α = 91.7°, β = 97.1°, γ = 102°; monoclinic γ-$(ET)_3(ReO_4)_2$: a = 16.3 Å, b = 12.01 Å, c = 12.42 Å, β = 91.2°. All three structures were reported to contain layers of ET molecules.

(34) Shibaeva, R. P.; Kaminskii, V. F.; Yagubskii, E. B. *Mol. Cryst. Liq. Cryst.* **1985**, *119*, 361.

(35) Wang, H. H.; Montgomery, L. K.; Husting, C. A.; Vogt, B. A.; Williams, J. M.; Budz, S. M.; Lowry, M. J.; Carlson, K. D.; Kwok, M.-K.; Mikjeyev, V. *Chem. Mater.* **1989**, *1*, 484.

electrochemical conditions influence the nucleation pathways in these systems.

Cyclic voltammetry of ET with polycrystalline platinum electrodes in acetonitrile reveals two reversible one-electron oxidations (eqs 1 and 2), in agreement with previous reports.[23,36] Anodic oxidation of I_3^- (eq 3) occurs at a potential near the second oxidation step of ET. The oxidation of both ET and I_3^- at a freshly cleaved HOPG electrode (Figure 2) occurs at potentials similar to those observed at platinum electrodes, although with slightly less electrochemical reversibility. The reduced reversibility is typical of redox processes at highly crystalline graphite and generally is attributed to slow kinetics at the exposed basal plane.[37]

	vs Ag/AgCl		
$ET^\circ \rightarrow ET^+ + e^-$	$E_0 = 0.65$	[peak A]	(1)
$ET^+ \rightarrow ET^{2+} + e^-$	$E_0 = 0.89$ V		(2)
$2I_3^- \rightarrow 3I_2 + e^-$	$E_0 = 0.86$ V	[peak B]	(3)
$2(ET) + I_3^- \rightarrow (ET)_2I_3 + e^-$	$E_{cryst} \approx 0.65$ V		(4)
$3I_2 + 2e^- \rightarrow 2I_3^-$	$E' = 0.80$ V	[peak C]	(5)
$ET^+ + e^- \rightarrow ET$	$E' = 0.67$ V	[peak D]	(6)
$(ET)_2I_3 + e^- \rightarrow 2(ET) + I_3^-$	$E' = 0.62$ V	[peak E]	(7)
$(ET)_2I_3$ (overlayer) $+ e^- \rightarrow 2(ET) + I_3^-$	$E' = 0.89$ V	[peak F]	(8)

Cyclic voltammetry performed with a cleaved HOPG electrode in acetonitrile containing *both* ET and I_3^- (Figure 3c) revealed the oxidation of both ET (peak A) and I_3^- (peak B) during the anodic potential excursion. Crystallization of $(ET)_2I_3$ occurs after electrochemical oxidation of ET (eq 4) at the foot of the I_3^- oxidation wave. Although the concentration of I_2 at the electrode surface is not substantial, I_2-mediated oxidation of ET cannot be ruled out at this potential.[38] Reversal of the potential scan following excursions into the I_3^-/I_2 couple resulted in four reduction peaks. The first (peak C) corresponded to the reduction of I_3^- (eq 5). This was followed by a shoulder and a peak at slightly more cathodic potentials, corresponding to the reduction of free ET^+ remaining in the depletion layer near the electrode surface (peak D, eq 6) and reduction of bulk $(ET)_2I_3$ on the electrode surface (peak E, eq 7), respectively. The assignment of peak E was corroborated by the observation that scanning the potential at a faster rate, which decreased the time available for crystallization, resulted in a decrease in the magnitude of peak E and a corresponding increase in peak D. Notably, a fourth reduction peak (peak F) was observed at potentials less positive than that of bulk $(ET)_2I_3$ dissolution *and* $(ET)_2I_3$ crystallization. Integration of the current under this peak indicated a coverage of $\Gamma_{(ET)_2I_3} = 2.4 \times 10^{-10}$ mol cm^{-2}, approaching the values expected for a (001)-like monolayer of α-$(ET)_2I_3$ ($\Gamma_{(ET)_2I_3} = 3.4 \times 10^{-10}$ mol cm^{-2}) or a (001)-like monolayer of β-$(ET)_2I_3$ ($\Gamma_{(ET)_2I_3} = 2.9 \times 10^{-10}$ mol cm^{-2}). In each case the ET molecules are nominally normal to the HOPG surface.[39] The position of this peak indicates that the monolayer is thermodynamically more stable than the bulk material, a characteristic typically assigned to underpotential deposited layers.[40] However, a prewave corresponding to monolayer formation during the anodic scan, preceding bulk ET oxidation, was never observed. This is consistent with slow kinetics for the formation of the underpotential deposited monolayer of $(ET)_2I_3$.

Atomic Force Microscopy of Overlayer Formation. The formation of ET-based monolayers was examined by real-time in situ atomic force microscopy (AFM) experiments performed with a freshly cleaved HOPG electrode immersed in an acetonitrile solution containing ET and I_3^- or ReO_4^-. In the presence of I_3^- application of a potential slightly anodic of E_{cryst} (>0.65 V vs Ag/AgCl) resulted in the formation of $(ET)_2I_3$ islands at random locations on terraces of the HOPG substrate surface, with each island exhibiting a height of 15.5 ± 0.5 Å. These islands grew anisotropically along preferred growth directions on the HOPG surface, with growth of an island eventually terminating either at the boundary of another island or at the edge of a graphite step (corresponding to a principal $\{\bar{1}2\bar{1}0\}$ lattice vector in the HOPG surface). The angles subtended by these preferred directions with the graphite steps observed in the image frame were 10 ± *n*60°. Eventually, these islands coalesced into a completely formed $(ET)_2I_3$ overlayer with a thickness of 15.5 Å.

AFM images acquired on small regions either within the $(ET)_2I_3$ islands or on the coalesced overlayer revealed molecular scale contrast with an ordered, periodic structure (Figure 4). The observation of lattice images indicate that the layer is crystalline and robust with respect to mechanical perturbation by the tip under these conditions.[41] The lattice parameters deduced from the real space and Fourier data revealed a 2-D unit cell with the lattice parameters $b_1 = 6.2 \pm 0.5$ Å, $b_2 = 9.4 \pm 0.8$ Å, and $\beta = 107 \pm 4°$. These values compare favorably to the single-crystal X-ray parameters of the (001) plane of bulk β-$(ET)_2I_3$, for which $a = 6.6$ Å, $b = 9.1$ Å, and $\gamma = 110°$. The 15.5 Å overlayer thickness is equivalent, within experimental error, to the thickness of the (001) layer in bulk β-$(ET)_2I_3$ ($d_{001} = 15.28$ Å). Notably, the overlayer lattice parameters and thickness do not correspond to the (001) layer in α-$(ET)_2I_3$ ($a = 9.183$ Å, $b = 10.804$ Å, $\gamma = 90.85°$, $d_{001} = 17.4$ Å) nor to any other crystallographic plane in either phase. These data clearly indicate that the $(ET)_2I_3$ overlayer formed on HOPG possesses an ordered structure which mimics the (001) layer in bulk β-$(ET)_2I_3$. Overlayers with this orientation, in which the long axes of the ET molecules are nominally perpendicular to the substrate, are designated herein as type I.

Further AFM experiments revealed that, upon continued application of an anodic potential exceeding E_{cryst}, bulk crystals of β-$(ET)_2I_3$ grew directly from the (001) overlayers via screw dislocations. These dislocations

(36) Sakura, S.; Imai, H.; Anzai, H.; Moriya, T. *Bull. Chem. Soc. Jpn.* **1988**, *61*, 3181.

(37) McCreery, R. L. In *Electroanalytical Chemistry: A Series of Advances*; Bard, A. J., Ed.; Marcel Dekker: New York, 1991; Vol. 17, p 303.

(38) (a) Endres, H.; Hiller, M.; Keller, H. J.; Bender, K.; Gogu, E.; Heinen, I.; Schweitzer, *Z. Naturforsch.* **1985**, *40b*, 1664. (b) Shibaeva, R. P.; Kaminskii, V. F.; Yagubskii, E. B. *Mol. Cryst. Liq. Cryst.* **1985**, *119*, 361.

(39) The theoretical coverage for a monolayer was based on the surface density of ET molecules on the (001) planes of α-$(ET)_2I_3$ and β-$(ET)_2I_3$, which reveals an average area per ET molecule of 25 Å^2 and 28 Å^2, respectively.

(40) Gregory, B. W.; Norton, M. L.; Stickney, J. L. *J. Electroanal. Chem.* **1990**, *293*, 85.

(41) Hutter, J. L.; Bechhoefer, J. *J. Appl. Phys.* **1993**, *73*, 4123.

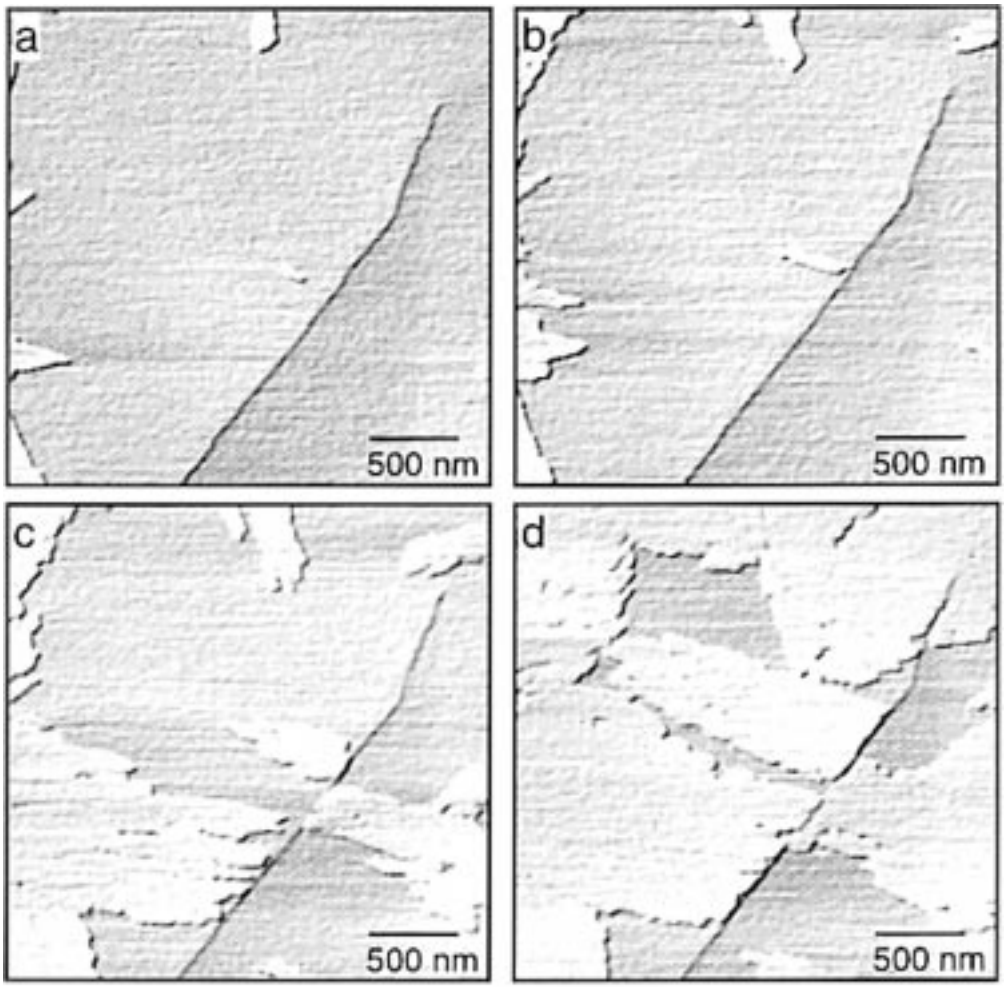

Figure 3. In situ AFM images acquired during electrochemical growth of the type I β-$(ET)_2I_3$ (001) overlayer on a freshly cleaved HOPG electrode at (a) $t = 30$, (b) 90, (c) 150, and (d) 210 s following a potential step to $E_{cryst} = 650$ mV (vs Ag/AgCl). The linear feature on the HOPG surface in the middle of each image corresponds to one of the $\{\bar{1}2\bar{1}0\}$ principal lattice vectors of HOPG ($\mathbf{a_1}$ or $\mathbf{a_2}$).

formed at the intersection of substrate steps, which argues that defects in the substrate were responsible for their formation. Individual β-$(ET)_2I_3$ layers emanate from these screw dislocations, leading to layer-by-layer growth of β-$(ET)_2I_3$ microcrystals (Figure 4). These microcrystals were identified readily as β-$(ET)_2I_3$ by their distinct morphology and by the lattice parameters of the large crystal face parallel to the HOPG substrate, which were identical with those of the (001) plane of β-$(ET)_2I_3$. These data demonstrate that the formation of the (001) β-$(ET)_2I_3$ overlayer is the source of the polymorph selectivity toward bulk β-$(ET)_2I_3$ on HOPG electrodes. The observation of the molecularly thick overlayer formed at lower potentials than required for bulk crystal growth is characteristic of a Stranski–Krastanov mechanism,[42] in which the monolayer–substrate interaction is greater than that between bulk layers.

The anisotropic growth of the (001) overlayer indicated by the 60° angle between preferred growth directions suggested a unique azimuthal orientation of the β-$(ET)_2I_3$ overlayer with respect to the HOPG substrate. An overlayer-substrate interface can be described by the

Scheme 1

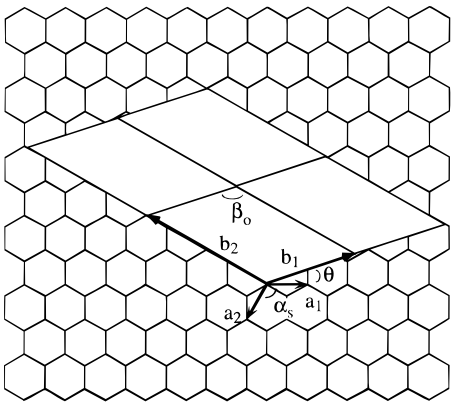

substrate lattice constants $\mathbf{a_1}$, $\mathbf{a_2}$, and α_s, the overlayer lattice constants $\mathbf{b_1}$, $\mathbf{b_2}$, and β_0, and the azimuthal orientation θ, defined as the angle between $\mathbf{a_1}$ and $\mathbf{b_1}$ (Scheme 1). In the case of HOPG, the substrate lattice vectors $\mathbf{a_1}$ and $\mathbf{a_2}$ correspond to the $[\bar{1}2\bar{1}0]$ and $[2\bar{1}\bar{1}0]$ directions. The value of θ for the β-$(ET)_2I_3$ overlayer on HOPG was determined by simultaneously acquiring lattice images of the overlayer and substrate. The substrate lattice images were acquired on regions of exposed substrate adjacent to the edges of an incompletely formed overlayer or on substrate regions exposed

(42) Stranski, I. N.; Krastanov, L. *Sitzungsber. Akad. Wiss. Wien, Math.–Naturwiss., Kl IIb* **1938**, *146*, 797.

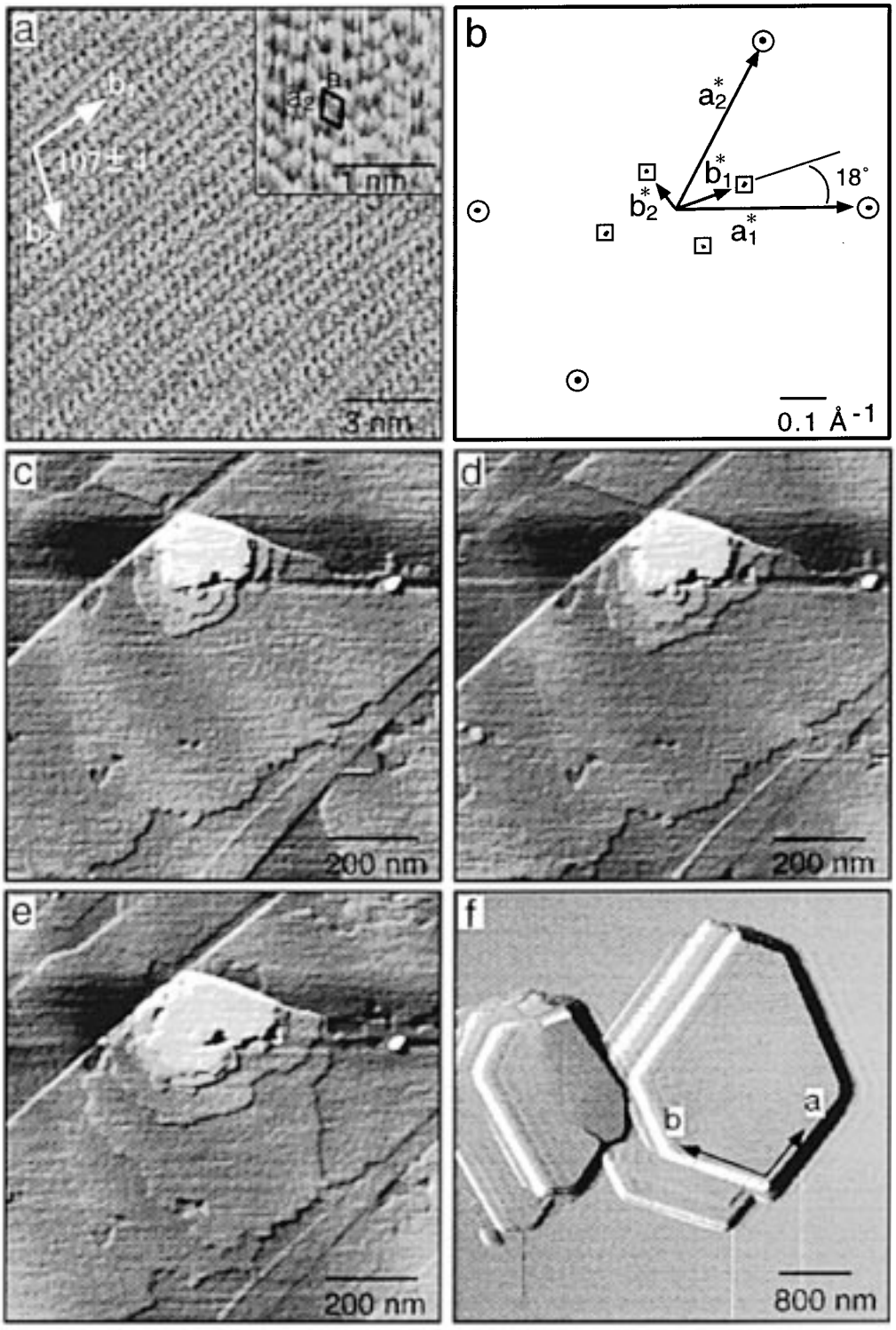

Figure 4. (a) AFM lattice image of the type I β-$(ET)_2I_3$ (001) overlayer acquired in situ under growth conditions. The overlayer lattice vectors illustrate only their direction and their lengths do not correspond to their actual magnitude. The lattice parameters determined from the real space and Fourier data are $b_1 = 6.2 \pm 0.5$ Å, $b_2 = 9.4 \pm 0.8$ Å, and $\beta = 107 \pm 4°$. Inset: lattice image of HOPG substrate directly below β-$(ET)_2I_3$ overlayer The unit cell defined by the lattice vectors $\mathbf{a}_1$ and $\mathbf{a}_2$ is superimposed. (b) Fourier spectra of the β-$(ET)_2I_3$ (001) overlayer and the HOPG substrate illustrating the relationship between the reciprocal lattice vectors $\mathbf{a}_1$*, $\mathbf{a}_2$* of HOPG (circles) and $\mathbf{b}_1$*, $\mathbf{b}_2$* of the β-$(ET)_2I_3$ overlayer (squares). These data reveal that the lattice vectors $\mathbf{a_1}$ and $\mathbf{b_1}$ subtend an angle of $\theta = 18°$. (c−e) AFM images showing the progressive layer-by-layer growth of a type I β-$(ET)_2I_3$ (001) multilayer in which the layers emanate by step flow from a screw dislocation. (f) AFM image of a microscopic crystal of β-$(ET)_2I_3$ grown on HOPG from the type I overlayer. Lattice images acquired by AFM confirmed that the large upper face was (001) with the crystallographic *a* and *b* axes oriented as shown. The *a* and *b* axes here have the same magnitude and orientation with respect to the HOPG substrate as $\mathbf{b_1}$ and $\mathbf{b_2}$ of the overlayer, respectively. The angle subtended by the *a* axis and the observed HOPG step is 40°, which is equivalent to 20° with a HOPG lattice vector that is 60° from the step. The morphology of this crystal is identical with that of larger β-$(ET)_2I_3$ crystals.

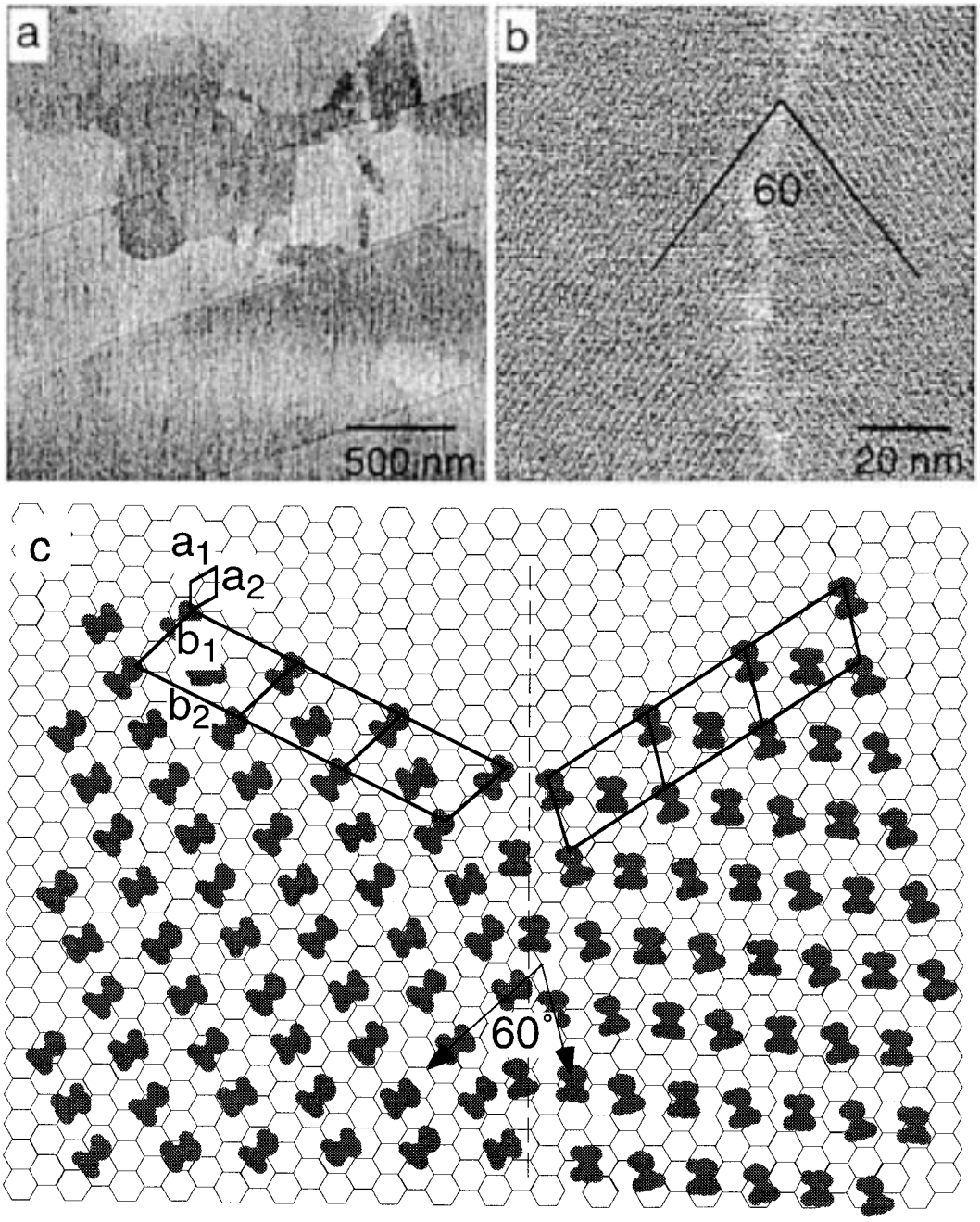

Figure 5. (a) Lateral force AFM image of a completely formed type I β-$(ET)_2I_3$ monolayer acquired at a scan angle = 0°, in which the scan direction is parallel to the long axis of the cantilever. The different contrast of the domain surfaces is due to the different $\pm n60°$ orientations of the overlayers as allowed by the 3-fold symmetry of the HOPG substrate. (b) AFM image of the boundary region between two adjoining domains. The lattices of the two domains are related by a 60° azimuthal rotation. Solid lines parallel to $\mathbf{b_1}$ are included as a visual aid to illustrate the different orientations. (c) An idealized representation of the two adjacent β-$(ET)_2I_3$ domains on an HOPG substrate with the domain boundary indicated by a dashed line. Only the ethylene ends of the ET molecules, which are presumed to be in contact with the HOPG surface, are shown for clarity.

by mechanical removal of the overlayer with the AFM tip. The latter was accomplished by rastering the AFM tip over this region at a higher force ($F_{app} \geq 20$ nN) than that used for imaging ($F_{image} \leq 5$ nN). Either method enabled simultaneous determination of θ and the overlayer lattice parameters. Comparison of the overlayer and substrate reciprocal lattice vectors in the Fourier data (Figure 4) indicated that $\theta = 18° \pm 3°$. Notably, the angle between $\mathbf{a_1}$ and the *a*-axis of the bulk β-$(ET)_2I_3$ single crystals grown from this monolayer was 18°. This demonstrates that, in addition to the normal orientation, the azimuthal orientation also is established at the overlayer stage of crystallization and is preserved during growth of the bulk crystal from the monolayer.

The coalescence of the separately growing domains during overlayer formation resulted in boundaries between domains which exhibited azimuthal orientations differing by $n60°$ (Figure 5). Lateral force imaging performed over large overlayer areas, in which the AFM tip was scanned perpendicular to the cantilever axis (scan angle = 90°), revealed increased cantilever twisting at the domain boundaries. This can be attributed to liquid-like disorder in these regions, which results in deeper penetration by the tip and a corresponding

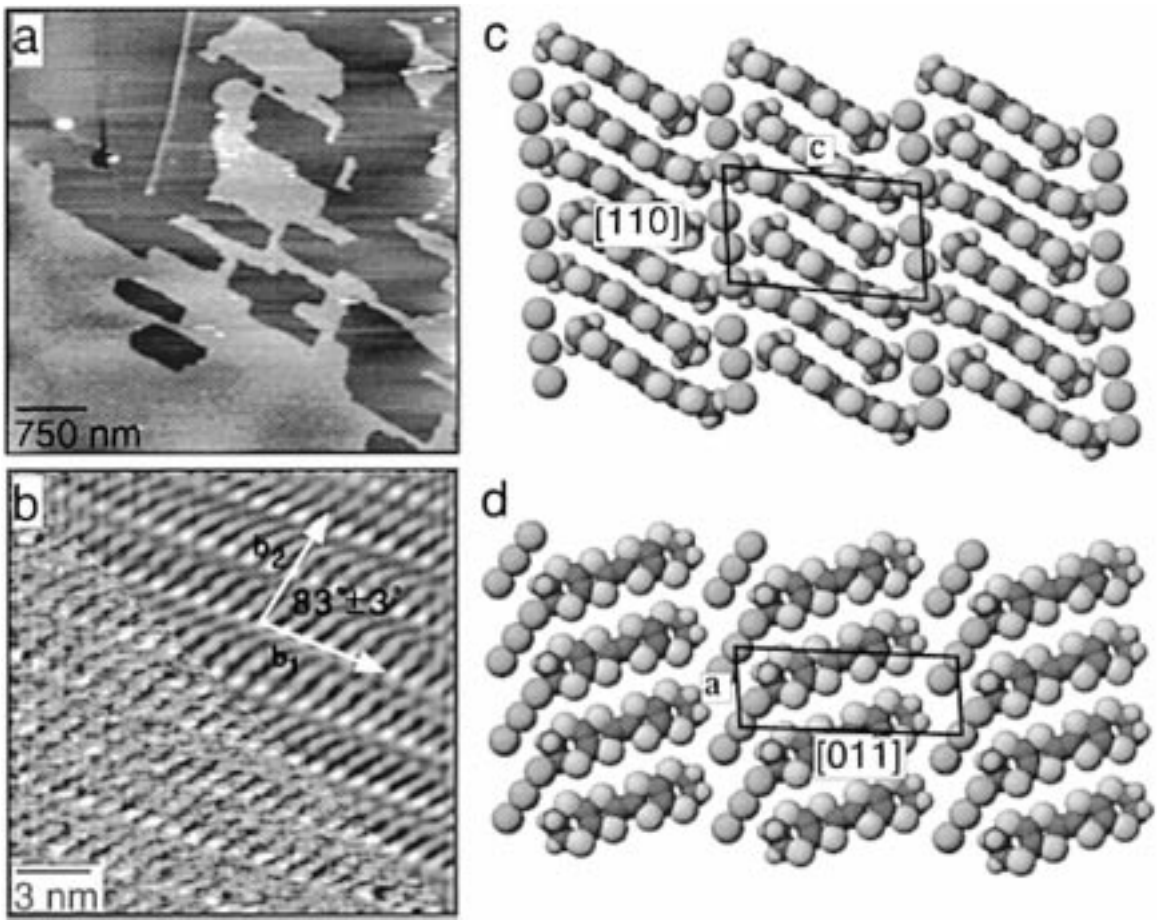

Figure 6. (a) In situ AFM image acquired during electrochemical growth of a type II β-$(ET)_2I_3$ overlayer on freshly cleaved HOPG following a potential step to E_{cryst} = 650 mV (vs Ag/AgCl). (b) High-resolution image of type II β-$(ET)_2I_3$ overlayer. The overlayer lattice vectors illustrate only their direction and their lengths do not correspond to their actual magnitude. The lattice parameters determined from the real space and Fourier data are $b_1 = 7.2 \pm 0.8$ Å, $b_2 = 17.3 \pm 1.8$ Å, and $\beta = 83 \pm 3°$. (c) Normal view of the packing in the $(\bar{1}10)$ plane of β-$(ET)_2I_3$. (d) Normal view of the packing in the (011) plane of β-$(ET)_2I_3$. The experimentally measured height of the type II film (6.3 Å) and the retention of $\pi-\pi$ stacking interactions argue that the overlayer is best described as a slightly reconstructed $(\bar{1}10)$ layer as in (c).

increase in cantilever twist (typically interpreted as increased friction). Lateral force images acquired with the tip motion *parallel* to the cantilever axis (scan angle = 0°) revealed different levels of friction among the domain *surfaces*. The observation of friction differences in this scanning mode was somewhat surprising but is indicative of different amounts of cantilever twist as the tip experiences differently oriented molecular fields on the β-$(ET)_2I_3$ (001) domain surfaces. The observation of different friction levels for the differently oriented domains with identical composition and structure indicates that the overlayer must be highly crystalline and rigid under these conditions. These domain boundaries can be annealed into large, defect-free areas ($>15\ \mu m^2$) by cycling the applied potential between the deposition and dissolution potentials.[43]

Occasionally, an overlayer with a structure differing from that of the β-$(ET)_2I_3$ (001) overlayer was observed during electrocrystallization on HOPG. This overlayer, designated as type II, grew as either a monolayer or a bilayer and was highly faceted (Figure 6). The facets subtended angles of 16° with the HOPG $\mathbf{a_1}$ lattice vector and typically were oriented along two well-defined directions within the overlayer, suggestive of crystalline order. The heights of the monolayer and bilayer were 6.3 ± 0.3 and 12.6 ± 0.6 Å, making this overlayer easily distinguishable from the type I overlayer and suggesting that the ET molecules were aligned with their short molecular axes perpendicular to the HOPG surface. Images acquired by AFM on small regions of the type II overlayer revealed an ordered 2-D lattice with constants of $b_1 = 7.2 \pm 0.8$ Å, $b_2 = 17.3 \pm 1.8$ Å, and $\beta_0 = 83 \pm 3°$.

The lattice parameters of the type II β-$(ET)_2I_3$ overlayer do not correspond exactly to any crystallographic plane in bulk β-$(ET)_2I_3$, but they approach the values describing both the $(\bar{1}10)$ and (011) planes in the bulk crystal. The lattice constants of the $(\bar{1}10)$ plane are c = 15.28 Å ($\approx 2b_1$) and ab (=[110]) = 9.26 Å ($\approx b_2/2$), with a layer height of approximately 6.6 Å and an 81.36° angle between these vectors. The observation of halved and doubled periodicites with AFM is not uncommon owing to the complexity of the ensemble imaging mechanism in which molecular contrast is the result of forces between the periodic molecular surface and the macroscopic tip. The ET molecules in the $(\bar{1}10)$ plane are stacked by $\pi-\pi$ charge-transfer interactions along [110]. The lattice constants of the (011) plane are a = 6.615 Å ($\approx b_1$) and $[01\bar{1}]$ = 18.38 Å ($\approx b_2$), with a layer height of approximately 4.5 Å and an angle of 82° between these

(43) Last, J. A.; Ward, M. D. *Adv. Mater.* **1996**, *8*, 730.

vectors. This plane consists of ET molecules organized along *a* by strong S···S interactions between neighboring ET molecules. On the basis of the measured overlayer heights, which can be determined more precisely than lattice parameters, and the premise that ET molecules would prefer to organize in a manner that preserves the strong $\pi-\pi$ configuration interactions between partially charged ET molecules, it is reasonable to assign the type II overlayer to a slightly reconstructed version of a β-$(ET)_2I_3$ $(\bar{1}10)$ layer in which the short molecular axis of ET is perpendicular to the HOPG surface. Comparison of the real space and Fourier data of the type II overlayer and underlying HOPG lattice revealed that the angle between $\mathbf{b_1}$ of the overlayer and $\mathbf{a_1}$ of HOPG was $\theta = 15 \pm 3°$. The $\mathbf{b_1}$ vector coincided with the edges of the facets observed in the partially grown monolayer.

Real-time in situ AFM also revealed growth of a molecular overlayer upon application of a potential sufficient to oxidize ET in the presence of n-$Bu_4N^+ReO_4^-$ (Figure 7). Overlayer growth occurred by formation of several faceted $(ET)_2ReO_4$ islands on the HOPG surface, with the facets oriented at $38 \pm n60°$ with respect to the HOPG step. These islands grew independently and eventually coalesced into a monolayer which completely covered the HOPG surface. The completely formed monolayer contained domains related by $\pm n60°$ azimuthal rotations. The overlayer height was 6.7 ± 0.4 Å, suggesting that the ET molecules were oriented with the short molecular axis perpendicular to the HOPG surface. Lattice images acquired on small regions of the overlayer indicated that the $(ET)_2ReO_4$ monolayer was crystalline, with lattice parameters of $b_1 = 7.1 \pm 0.3$ Å, $b_2 = 19.8 \pm 0.6$ Å, and $\beta = 103 \pm 5°$. Comparison of the lattice images of the overlayer and HOPG substrate revealed that $\theta = 34 \pm 4°$. Examination of bulk crystal planes containing the long molecular axis of ET suggests that the overlayer most closely resembles the (011) plane of $(ET)_2ReO_4$, in which the short molecular axes of the ET molecules are nominally normal to the plane. The thickness of the (011) layer is 5.7 Å and the lattice constants within the plane are $a = 7.78$ Å and $[01\bar{1}] = 17.9$ Å, these two vectors subtending an angle of 98.8°. The facets observed in the overlayer during growth correspond to $\mathbf{b_1}$, which in turn corresponds to the [100] direction in the (011) layer.

Overlayer−Substrate Interface. The AFM data indicate that the overlayers are 2-D crystalline assemblies described by two lattice vectors $\mathbf{b_1}$ and $\mathbf{b_2}$, and the angle β_0. These overlayers exhibit unique azimuthal orientations that suggest free-energy minima resulting from epitaxial ordering of the overlayer on the HOPG substrate. These molecular lattices have lower symmetry than the HOPG surface, which prohibits strict commensurism that is commonly observed for inorganic and elemental thin films. Rather, it is more likely that molecular films will be either incommensurate or coincident. Although unique azimuthal orientations are not expected for incommensurate films, preferred azimuthal orientations are expected if the overlayer is coincident with the substrate. Coincidence exists if the overlayer and substrate each have a reciprocal lattice vector oriented along a common direction, with the magnitude of the overlayer reciprocal lattice vector being an integer multiple of the substrate reciprocal lattice vector. This affords a nonprimitive supercell consisting of an array of overlayer unit cells in which only the supercell *vertexes* exhibit strict "point-on-point" commensurism with the substrate. Noncommensurate overlayer sites contained within the boundaries of the supercell actually are related to the substrate by "point-on-line" coincidence in which the overlayer lattice sites sit on specific lattice vectors of the substrate.[44] Coincidence is energetically less favorable than commensurism if only the overlayer−substrate interactions are considered. Nevertheless, coincident epitaxy can exist if the intermolecular interactions within the overlayer are strong enough to resist reconstruction to a form that is purely commensurate with the substrate. We reported recently[25] that coincident epitaxy was responsible for the configuration of several robust low symmetry molecular overlayers grown on van der Waals substrates,[45] including overlayers on HOPG that had been characterized as "quasi-epitaxial".[46] Our analysis of recently published data also suggests that coincident epitaxy governs the configuration of overlayers based on hydrogen-bonded liquid crystals[47] and thiophene−alkylpyrrole oligomers.[48]

Analysis of a coincident overlayer−substrate interface and prediction of the most favorable configuration by direct potential energy calculations can be difficult because these calculations require large basis sets in order to establish the phase relationship between the potential functions of the two lattices. At a minimum, these basis sets must include the atoms contained within the supercell and the atoms of the HOPG surface in contact with the supercell. We recently reported a more computationally efficient procedure for analysis of the overlayer−substrate interface that uses a direct analytical function to analyze the misfit between the two lattices.[25] This procedure relies on a program written in our laboratory (EpiCalc) that calculates a dimensionless potential V/V_0. The value of V/V_0 assumes discrete values for incommensurate ($V/V_0 = 1.0$),

(44) van der Merwe, J. H. *Philos. Magn. A* **1982**, *45*, 127.

(45) (a) Collins, G. E.; Nebesny, K. W.; England, C. D.; Chau, L.; Lee, P. A.; Parkinson, B.; Fernando, Q.; Armstrong, N. R. *J. Vac. Sci. Technol. A* **1992**, *10*, 2902. (b) Armstrong, N. R.; Nebesny, K. W.; Collins, G. E.; Chau, L.-K.; Lee, P. A.; England, C. D.; Diehl, D.; Douskey, M.; Parkinson, B. *Thin Solid Films* **1992**, *216*, 90. (c) Nebesny, K. W.; Collins, G. E.; Lee, P. A.; Chau, L.-K.; Danziger, J.; Osburn, E.; Armstrong, N. R. *Chem. Mater.* **1991**, *3*, 829. (d) Ludwig, C.; Gompf, B.; Flatz, W.; Peterson, J.; Eisenmenger, W.; Mobus, M.; Zimmermann, U.; Karl, N. *Z. Phys. B* **1992**, *86*, 397. (e) Ludwig, C.; Gompf, B.; Peterson, J.; Strohmaier, R.; Eisenmenger, W. *Z. Phys. B* **1993**, *93*, 365.

(46) (a) Forrest, S. R.; Zhang, Y. *Phys. Rev. B* **1994**, *49*, 11297. (b) Zhang, Y.; Forrest, S. R. *Phys. Rev. Lett.* **1993**, *71*, 2765.

(47) Calculations performed in our laboratory suggest that a recently reported hydrogen-bonded liquid-crystal overlayer based on an alkylated isophthalic acid derivative (C_{16}IsA) on a HOPG substrate is coincident. STM data for C_{16}IsA: STM data: $b_1 = 9.3 \pm 0.15$ Å, $b_2 = 33 \pm 2$ Å, $\beta = 90° \pm 2° = \theta = 9°$ (estimated). Calculated: $b_1 = 9.45$ Å, $b_2 = 32.8$ Å, $\beta = 90°$, $\theta = 13°$, $m_{11} = 3.25$, $m_{12} = 1.0$, $m_{21} = -10.5$, $m_{22} = 15.0$; supercell size = $4\mathbf{b_1} \times 2\mathbf{b_2}$. See: Eichhorst-Gerner, K.; Stabel, A.; Moessner, G.; Declerq, D.; Valiyaveettil, S.; Enkelmann, V.; Mullen, K.; Rabe, J. P. *Angew. Chem., Int. Ed. Engl.* **1996**, *35*, 1492.

(48) Calculations performed in our laboratory suggest that recently reported overlayers assembled from thiophene−alkylpyrrole oligomers $SP_{12}SSP_{12}S$ and $SP_{12}SP_{12}SP_{12}S$ (S = thiophene, P_{12} = *N*-dodecylpyrrole) on a HOPG substrate is coincident. See: Wu, X.; Parakka, J. P.; Cava, M. P.; Kim, Y.-T.; Metzger, R. M. *Synth. Met.* **1995**, *71*, 2105. STM data for $SP_{12}SSP_{12}S$: $b_1 = 19 \pm 0.5$ Å, $b_2 = 8 \pm 0.3$ Å, $\beta = 90°$. Calculated: $b_1 = 18.6$ Å, $b_2 = 7.8$ Å, $\beta = 90°$, $\theta = 25°$, $m_{11} = 5$, $m_{12} = 3.66$, $m_{21} = -3.0$, $m_{22} = 3.33$; supercell size = $3\mathbf{b_1} \times 3\mathbf{b_2}$. STM data for $SP_{12}SP_{12}SP_{12}S$: $b_1 = 23 \pm 0.5$ Å, $b_2 = 18 \pm 0.5$ Å, $\beta = 90°$; Calculated: $b_1 = 22.7$ Å, $b_2 = 18.5$ Å, $\beta = 90°$, $\theta = 9.8°$, $m_{11} = 8.2$, $m_{12} = 1.8$, $m_{21} = -5.5$, $m_{22} = 8.5$; supercell size = $5\mathbf{b_1} \times 2\mathbf{b_2}$.

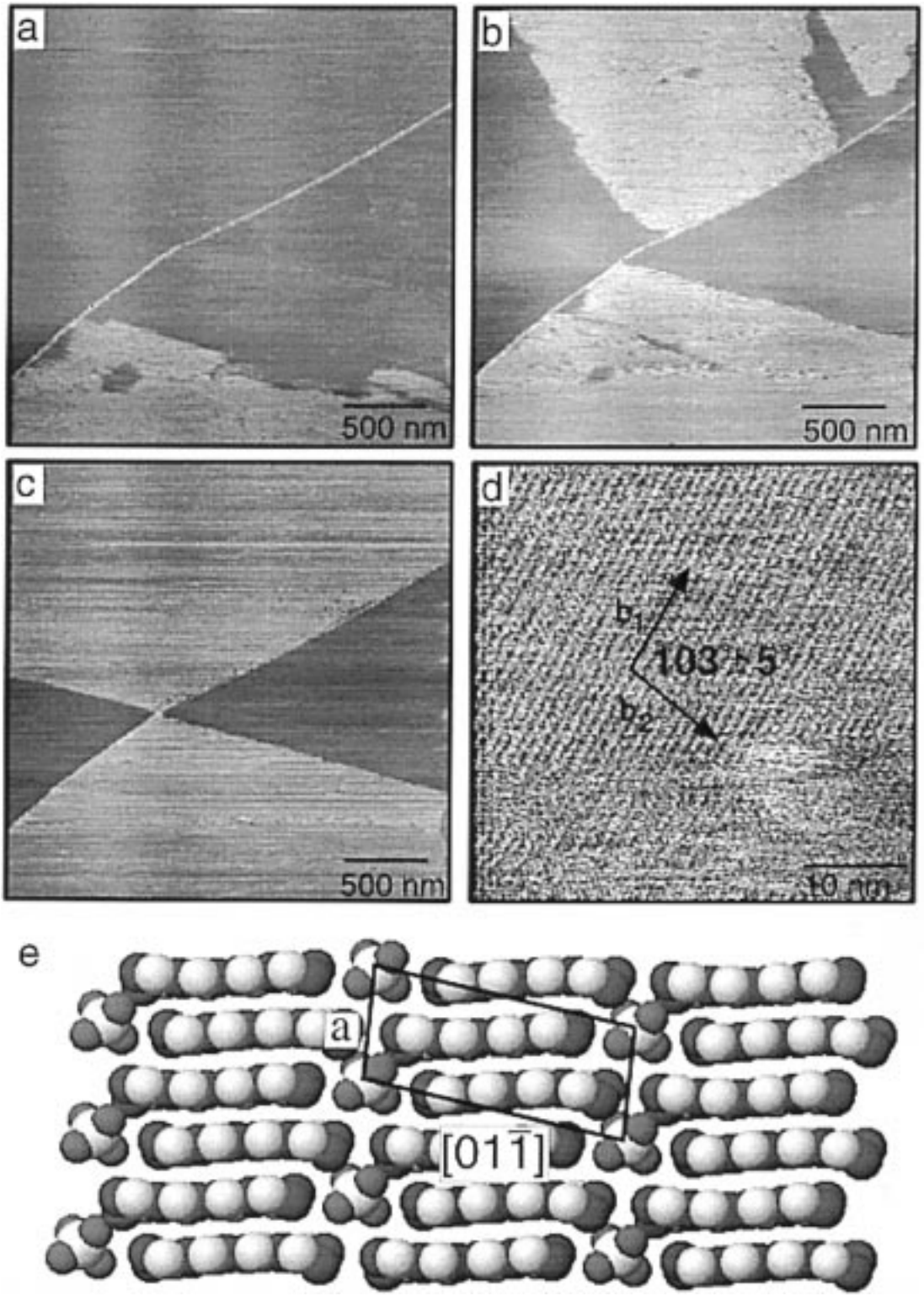

Figure 7. In situ AFM images acquired during growth of $(ET)_2ReO_4$ overlayer on a freshly cleaved HOPG electrode at (a) $t = 30$, (b) 60, and (c) 510 s following a potential step to 700 mV (vs Ag/AgCl). (d) Lattice image of the $(ET)_2ReO_4$ overlayer acquired by AFM in situ under growth conditions. The overlayer lattice vectors illustrate only their direction, and their lengths do not correspond to their actual magnitude. The lattice parameters determined from the real space and Fourier data are $b_1 = 7.1 \pm 0.3$ Å, $b_2 = 19.8 \pm 0.6$ Å, and $\beta = 103 \pm 5°$.

coincident ($V/V_0 = 0.5$) and commensurate ($V/V_0 = 0.0$) lattices. Calculation of V/V_0 for a given set of overlayer and substrate lattice parameters over a specified range of θ values reveals the mode of epitaxy and the optimum azimuthal angle for coincidence or commensurism, if these conditions exist. Unlike potential energy calculations, the computational time required by EpiCalc is independent of overlayer size. This is especially advantageous for coincident overlayers with large supercells as accurate determination of the optimum azimuthal angle requires a basis set corresponding to at least several supercells in order to establish the phase relationship between the supercell and the substrate lattice.[49]

Calculation of V/V_0 over the range $0 < \theta < 60°$ (which is sufficient for the HOPG surface) using the bulk α-$(ET)_2I_3$ (001) lattice parameters indicated only incommensurism. However, calculation of V/V_0 using the bulk β-$(ET)_2I_3$ (001) lattice parameters revealed coincidence with $V/V_0 = 0.5$ at $\theta = 19.8°$, essentially identical with the value of $\theta = 18°$ determined by AFM. This argues that coincident epitaxy governs overlayer formation and is the source of the polymorph selectivity observed for the growth of bulk β-$(ET)_2I_3$ crystals on HOPG. The β-$(ET)_2I_3$ (001) overlayer lattice is related to the HOPG lattice by the transformation matrix in eq 9. Alternatively, the overlayer lattice vectors can be expressed in terms of the substrate vectors according to eqs 10 and 11. This orientation results in overlayer lattice sites that exhibit point-on-line coincidence with the $\mathbf{a_2}$ lattice vector. The supercell size can be deduced from the value of an integer multiplier required to achieve an integral value for the coefficient preceding $\mathbf{a_2}$ in each equation. Consequently, the supercell of the β-$(ET)_2I_3$ (001) overlayer has dimensions of $1\mathbf{b_1} \times 3\mathbf{b_2}$ so that the supercell area is *3 times larger* than the area of the (001) unit cell. We note that coincidence with a $9\mathbf{b}_1 \times 1\mathbf{b}_2$ supercell can be achieved for a slightly reconstructed α-$(ET)_2I_3$ (001) overlayer, but this was never observed experimentally.[50]

$$\begin{bmatrix}\mathbf{b_1}\\ \mathbf{b_2}\end{bmatrix} = \begin{bmatrix}2.0 & 1.0\\ -4.0 & 3.3\end{bmatrix}\begin{bmatrix}\mathbf{a_1}\\ \mathbf{a_2}\end{bmatrix} \tag{9}$$

$$\mathbf{b_1} = 2.0\ \mathbf{a_1} + 1.0\ \mathbf{a_2} \tag{10}$$

$$\mathbf{b_2} = -4.0\ \mathbf{a_1} + 3.3\ \mathbf{a_2} \tag{11}$$

Calculation of V/V_0 for the bulk β-$(ET)_2I_3$ ($\bar{1}10$) and (011) planes on HOPG indicated incommensurism for both planes. In contrast, calculation of V/V_0 using the mean lattice parameters obtained from the AFM data for the β-$(ET)_2I_3$ type II overlayer indicated a coincident cell with $V/V_0 = 0.5$ at $\theta = 17°$. This azimuthal angle is identical, within error, to the value of $\theta = 15°$ measured by AFM. The resulting coincident lattice is described by point-on-line coincidence upon the $\mathbf{a}_1$ lattice vector. The supercell size deduced from the matrix coefficients is $3\mathbf{b}_1 \times 5\mathbf{b}_2$, giving a supercell area which is *15 times larger* than the primary overlayer unit cell area.

Calculation of V/V_0 using the parameters of the (001) layer of bulk $(ET)_2ReO_4$ indicated that coincidence with HOPG could be achieved at $\theta = 33.2°$, with point-on-line coincidence upon the $\mathbf{a_1}$ lattice vector and a $3\mathbf{b_1} \times 4\mathbf{b_2}$ supercell. Similar calculations for low index planes ($h < 2$, $k < 2$, $l < 2$) of the other polymorphs revealed coincidence for only the β-$(ET)_3(ReO_4)_2$ (010) plane, which was reported to have a highly one-dimensional structure. However, the AFM data argue against the formation of either a $(ET)_2ReO_4$ (001) or a β-$(ET)_3(ReO_4)_2$ (010) overlayer because the measured overlayer height of 6.7 Å is substantially less than the crystallographic layer thicknesses (16.97 and 16.11 Å, respectively). Rather, the overlayer height is consistent with an overlayer structure in which the short axis of the ET molecules is perpendicular to the surface, similar to the orientation observed in the 5.7 Å thick (011) plane of bulk $(ET)_2ReO_4$. Calculation of V/V_0 based on the mean lattice constants measured by AFM indicated point-on-line coincidence upon the $\mathbf{a_1}$ lattice vector with $V/V_0 = 0.5$ at $\theta = 36°$, in good agreement with the value of $\theta = 34°$ measured by AFM. The AFM data and these calculations suggest that the overlayer adopts a structure resembling a slightly reconstructed form of the bulk (011) layer in order to become coincident with the HOPG substrate. Calculation of V/V_0 using the bulk crystallographic (011) layer indicated incommensurism at all values of θ. The supercell dimensions of the reconstructed (011) overlayer are $3\mathbf{b_1} \times 1\mathbf{b_2}$, giving a supercell which is only *3 times larger* than the unit cell, substantially smaller than the supercell of the putative (001) overlayer.

Overlayer−Substrate Energetics. The agreement between the AFM measurements and the predicted azimuthal angles for the $(ET)_2I_3$ and $(ET)_2ReO_4$ overlayers demonstrates that coincident epitaxy governs the structure of these overlayers and their orientation on the HOPG surface. Coincidence provides a mechanism for lowering the energy of the overlayer in that the vertexes of the supercell are commensurate with the substrate (open circles in Figures 8−10). If these substrate sites are viewed as the most energetically favorable positions for overlayer lattice sites, overlayer molecules contained within the supercell must sit on noncommensurate sites (open squares in Figures 8−10) that are displaced from nearby energetically preferred sites. The overlayer−substrate interface energy could be lowered further by expanding the overlayer to the extent that all the molecules sit on substrate sites so that commensurism is attained. However, this would be accompanied by an energetic penalty associated with the loss of intermolecular interactions within the overlayer. The structure of the overlayer therefore will reflect the balance between the overlayer−substrate interactions and the intermolecular interactions within the overlayer.

The displacement of the noncommensurate positions within the coincident supercell from energetically ideal (commensurate) positions can be considered as a strain along the overlayer−substrate interface. Similarly, perturbations to the overlayer structure required to achieve commensurism or coincidence can be considered as a strain within the overlayer with respect to a native overlayer structure (assumed to be a corresponding layer structure in a bulk crystal). The likelihood of commensurate or coincident lattices can be surmised from the stresses at the overlayer−substrate interface resulting from these strained positions. If the strains are sufficiently small, the system can be described by a linear stress−strain relationship, which allows determination of the elastic constants associated with the overlayer−substrate interface and the overlayer lattice. These elastic constants, which represent the stiffnesses of the overlayer−substrate interface and the overlayer

(49) We demonstrated previously[25] that accurate determination of θ, by either potential energy calculations or V/V_0 determinations, requires large overlayers. For example, a single minimum at $\theta = 19°$ for the $(ET)_2I_3$ overlayer on HOPG became apparent only at overlayer sizes approaching $7\mathbf{b_1} \times 7\mathbf{b_2}$.

(50) The coincident reconstructed (001) α-$(ET)_2I_3$ overlayer has lattice parameters within 2% of the bulk parameters: $b_1 = 9.35$ Å, $b_2 = 10.74$ Å, $\beta = 90.85°$, $\theta = 5.75°$, $m_{11} = 3.56$, $m_{12} = 0.44$, $m_{21} = -3.0$, $m_{22} = 5.0$; supercell size = $9\mathbf{b_1} \times 1\mathbf{b_2}$.

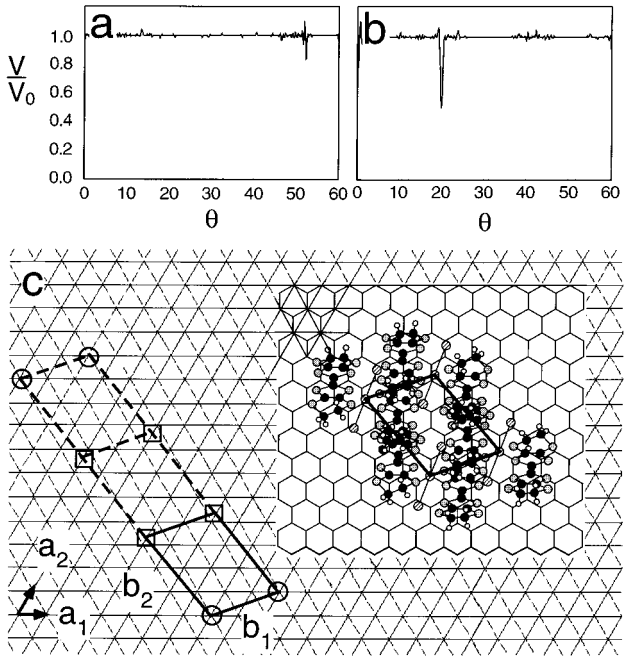

Figure 8. (a) Calculated dependence of V/V_0 on azimuthal angle θ for an α-$(ET)_2I_3$ (001) overlayer on the HOPG basal plane. The values of $V/V_0 = 0$ indicate the absence of coincidence and commensurism. (b) Calculated dependence of V/V_0 on azimuthal angle θ for a β-$(ET)_2I_3$ (001) overlayer on the HOPG basal plane. The value of $V/V_0 = 0.5$ at 19.8° indicates coincidence of the overlayer with the substrate. (c) Schematic representation of the type I (001) β-$(ET)_2I_3$ overlayer lattice on HOPG. The perimeter of the primitive overlayer unit cell is depicted by a solid line, and the perimeter of the nonprimitive $1\mathbf{b_1} \times 3\mathbf{b_2}$ supercell for the coincident overlayer is illustrated by the dashed line. The three principal lattice vectors of HOPG are depicted as solid lines. The open squares represent the overlayer lattice sites exhibiting point-on-line concidence, and the open circles define the supercell vertexes lying directly on substrate lattice sites with point-on-point coincidence. The right side of the figure illustrates the molecular motif of the type I β-$(ET)_2I_3$ (001) overlayer on a conventional representation of the HOPG surface.

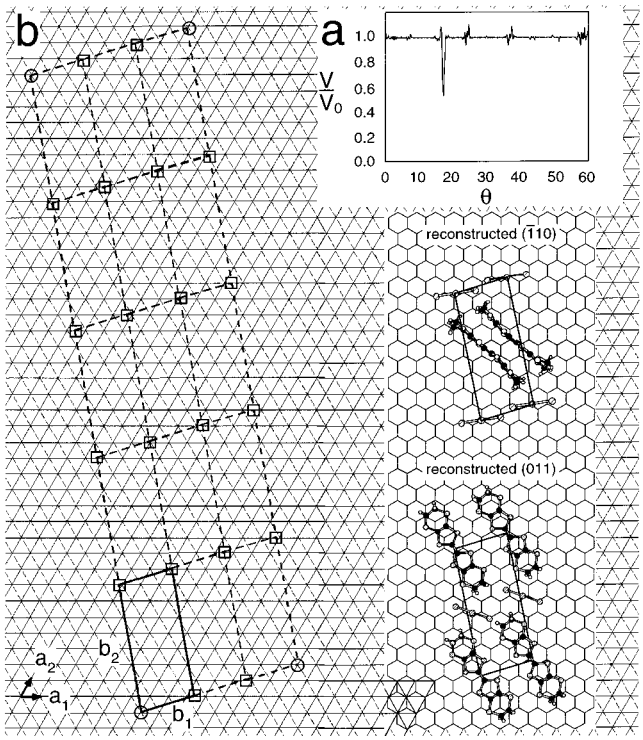

Figure 9. (a) Dependence of V/V_0 on azimuthal angle θ for a type II β-$(ET)_2I_3$ overlayer on the HOPG basal plane based on the overlayer lattice constants determined by AFM. The value of $V/V_0 = 0.5$ at $\theta = 17°$ indicates coincidence of the overlayer with the substrate. (b) Schematic representation of the type II ($\bar{1}10$) β-$(ET)_2I_3$ overlayer lattice on HOPG. The perimeter of the primitive overlayer unit cell is depicted by a solid line and the perimeter of the nonprimitive $3\mathbf{b_1} \times 5\mathbf{b_2}$ supercell for the coincident overlayer is illustrated by the dashed line. The three principal lattice vectors of HOPG are depicted as solid lines. The open squares represent the overlayer lattice sites exhibiting point-on-line concidence, and the open circles define the supercell vertexes lying directly on substrate lattice sites with point-on-point coincidence. The molecular motifs of the type II β-$(ET)_2I_3$ ($\bar{1}10$) and (011) overlayers on the HOPG surface are illustrated in the lower right of the figure.

along specified Cartesian coordinates, can be determined directly from the second derivative of the corresponding potential functions. The second derivative simply describes the curvature of a potential well, the elastic constant increasing with increasing curvature of the well. A large elastic constant is tantamount to a large energetic penalty associated with displacement from the energy minimum along a specified coordinate. Large overlayer−substrate elastic constants can result in substantial interfacial stresses for the noncommensurate positions in coincident lattices. The contribution from these stresses will increase as the supercell size required for coincidence becomes larger. Conversely, large intralayer elastic constants will result in large intralayer stresses if the overlayer structure changes significantly in order to achieve commensurism. Coincident lattices therefore will be favored for systems with small interfacial elastic constants and large intralayer elastic constants, provided a coincident configuration is possible for a particular overlayer−substrate combination. Under these conditions, the stresses associated with overlayer reconstruction to a commensurate form would be greater than those resulting from placing molecules on the noncommensurate sites within the supercell.

The interfacial elastic constants were determined by calculating the interfacial potential functions associated with translation of the overlayer along a principal HOPG lattice vector parallel to the interface and translation normal to the substrate (Table 2). These calculations were performed at the optimum azimuthal angle and at a constant mean overlayer-substrate separation, chosen as the minimum in the potential with respect to translation normal to the HOPG substrate (z-axis). The potential energies at these minima typically have small values because of weak physisorption (for example, $E_{min} = -15.1$ kcal mol^{-1} for β-$(ET)_2I_3$ (001) on HOPG). However, the potentials wells along z had rather high curvatures, which facilitated determination of the average minimum energy overlayer−substrate separations. The elastic constant c_{zz}^{inter} is associated with the strain ϵ_z and stress σ_z^{inter} normal to the overlayer−substrate interface along the z coordinate. The elastic constants $c_{a_1a_1}^{inter}$ and $c_{a_2a_2}^{inter}$ are associated with the strains ϵ_{a_1} and ϵ_{a_2}, and stresses $\sigma_{a_1}^{inter}$ and $\sigma_{a_2}^{inter}$, associated with the displacement of overlayer molecules along $\mathbf{a_1}$ and $\mathbf{a_2}$, respectively, from ideal positions (Scheme 2). The c_{zz}^{inter} values were large compared to $c_{a_1a_1}^{inter}$ and $c_{a_2a_2}^{inter}$, consistent with the high-curvature potential functions that generate the

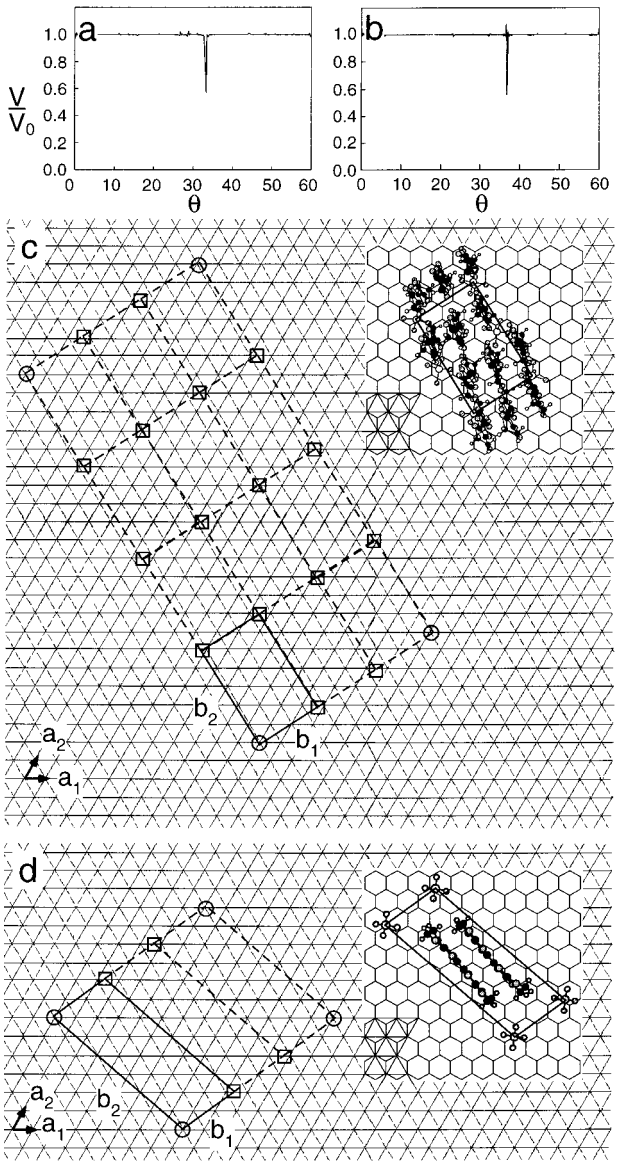

Figure 10. (a) Dependence of V/V_0 on azimuthal angle θ for a $(ET)_2ReO_4$ (001) overlayer on the HOPG basal plane. The value of $V/V_0 = 0.5$ at $\theta = 33.2°$ indicates coincidence of the overlayer with the substrate. (b) Dependence of V/V_0 on azimuthal angle θ for a type II β-$(ET)_2ReO_4$ (011) overlayer on the HOPG basal plane based on the overlayer lattice constants determined by AFM. The value of $V/V_0 = 0.5$ at $\theta = 36°$ indicates coincidence of the overlayer with the substrate. (c) Schematic representation of the crystallographic $(ET)_2ReO_4$ (001) lattice on HOPG. The perimeter of the primitive overlayer unit cell is depicted by a solid line and the perimeter of the nonprimitive $3\mathbf{b_1} \times 4\mathbf{b_2}$ supercell for the coincident overlayer is illustrated by the dashed line. The three principal lattice vectors of HOPG are depicted. (d) Schematic representation of the type II $(ET)_2ReO_4$ (011) overlayer lattice on HOPG based on the lattice constants corresponding to the coincident lattice of (b). The perimeter of the primitive overlayer unit cell is depicted by a solid line and the perimeter of the nonprimitive $1\mathbf{b_1} \times 3\mathbf{b_2}$ supercell for the coincident overlayer is illustrated by the dashed line. The three principal lattice vectors of HOPG are depicted. In (c) and (d) the open squares represent the overlayer lattice sites exhibiting point-on-line concidence, and the open circles define the supercell vertexes lying directly on substrate lattice sites with point-on-point coincidence. The molecular motifs of the overlayers on a conventional representation of the HOPG surface are illustrated in the upper right of each figure.

Scheme 2

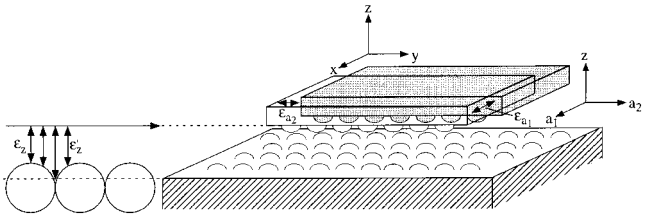

former. The elastic constants $c_{a_1z}^{inter}$ and $c_{a_2z}^{inter}$ are associated with the stress σ_z^{inter} along the z coordinate which results from local changes in overlayer−substrate separations as these corrugated surfaces are displaced along $\mathbf{a_1}$ and $\mathbf{a_2}$, respectively, at a constant mean overlayer−substrate separation (Scheme 2). The intralayer energies were calculated using a Lennard-Jones 6−12 potential function over a range of lattice dimensions by compressing and expanding the overlayer about the dimensions of the corresponding layer structure from the three-dimensional bulk crystal (see Experimental Section).[51] The intralayer elastic constants c_{xx}^{intra} and c_{yy}^{intra} represent the resistance of the overlayer toward structural perturbation away from the minimum energy configuration along specific crystallographic directions (these directions may correspond to either principal or nonprincipal axes in the crystallographic layer).

Analysis of the elastic constants for the systems described here suggest conditions that are favorable for coincident lattices. The calculated minimum energy structure for the close-packed β-$(ET)_2I_3$ (001) layer is essentially identical with that observed in the bulk crystal, with only a slight 0.06 Å lengthening along a and a negligible 0.01 Å compression along b. This illustrates that the structure of this layer is governed primarily by two-dimensional interactions ($\pi-\pi$ charge-transfer and dispersive S···S interactions) and is influenced only weakly by interactions between layers in the crystal. These strong intermolecular interactions are accompanied by intralayer elastic constants for extensional strain along a and b that are nearly an order of magnitude larger than the elastic constants associated with the overlayer−HOPG interface. Consequently, the energetic penalty from ET molecules sitting on noncommensurate sites within the coincident supercell instead of commensurate sites is smaller than the energy penalty that would accompany expansion of the overlayer to a commensurate form. The β-$(ET)_2I_3$ (001) overlayer requires no reconstruction from its native crystallographic structure to become coincident and the small supercell size minimizes the energetically unfavorable noncommensurate positions. Conversely, the

(51) In the case of β-$(ET)_2I_3$ (001) and $(ET)_2ReO_4$ (001) the layer structures in the corresponding bulk crystals were essentially identical with the calculated energy minimum for each layer; this agreement can be attributed to the strong 2-D interactions in these layers. Slight differences between the crystallographic and calculated layer structures were observed for the β-$(ET)_2I_3$ (011), β-$(ET)_2I_3$ ($\bar{1}$10) and $(ET)_2ReO_4$ (011) layers. Lattice parameters for the minimum energy configurations of β-$(ET)_2I_3$ and $(ET)_2ReO_4$ layers were calculated with a Lennard-Jones potential. These values can be compared with the crystallographic bulk values provided in Table 1. β-$(ET)_2I_3$ (001): (a_{min} = 6.67 Å, b_{min} = 9.09 Å; β = 110°); β-$(ET)_2I_3$ (011): (a_{min} = 6.65 Å, $[01\bar{1}]_{min}$ = 18.6 Å; β = 83°); β-$(ET)_2I_3$ (110): (a_{min} = 9.20 Å, $[110]_{min}$ = 15.10 Å; β = 81°); $(ET)_2ReO_4$ (001): (a_{min} = 7.70 Å, b_{min} = 12.69 Å; β = 87°); $(ET)_2ReO_4$ (011): (a_{min} = 7.80 Å, $[01\bar{1}]_{min}$ = 17.6 Å; β = 101°).

Table 1. Single Crystal X-ray Crystallographic Lattice Parameters for $(ET)_2X$ Salts and Measured AFM Lattice Parameters[a]

					AFM data		
compound	X-ray lattice parameters				overlayer parameters		azimuthal angle (θ) obs/calc[c]
β-ET_2I_3 ($P\bar{1}$)[ref]	*a*	**6.62 Å**	α	94.4°	b_1	6.2 ± 0.5 Å	18°/19.8°
	b	**9.10 Å**	β	95.5°	b_2	9.4 ± 0.8 Å	
	c	15.28 Å	γ	**109.8°**	β_0	107 ± 4°	
					overlayer height	15.5 ± 0.5 Å (*c*)	
β-$(ET)_2I_3$ ($P\bar{1}$) (011) overlayer	*a*	**6.615 Å**			b_1	7.2 ± 0.8 Å	15°/17°
	[**01**$\bar{1}$]	**18.38 Å**			b_2	17.3 ± 1.8 Å	
			ϕ[b]	**82°**	β_0	83 ± 3°	
	layer height	4.5 Å			overlayer height	6.3 ± 0.3 Å	
β-$(ET)_2I_3$ ($P\bar{1}$)($\bar{1}$10) overlayer	c	**15.28 Å**			b_1	7.2 ± 0.8 Å	15°/17°
	[110]	**9.26 Å**			b_2	17.3 ± 1.8 Å	
			ϕ[b]	**81.36°**	β_0	83 ± 3°	
	layer height	6.6 Å			overlayer height	6.3 ± 0.3 Å	
$(ET)_2ReO_4$ ($P\bar{1}$)[ref]	*a*	**7.78 Å**	α	73.01°	b_1	7.1 ± 0.3 Å	34°/36°
	b	12.59 Å	β	79.89°	b_2	19.8 ± 0.6 Å	
	c	16.97 Å	γ	89.06°	β_0	103 ± 5°	
	[**01**$\bar{1}$]	**17.9 Å**	ϕ[b]	**98.8°**			
	layer height	5.7 Å			overlayer height	6.7 ± 0.4 Å	

[a] Bolded X-ray lattice parameters correspond to those that best fit the overlayer lattice parameters determined by AFM. [b] ϕ is the angle between the vectors highlighted in bold. [c] Calculated azimuthal angles were determined with Epicalc.

Table 2. Overlayer Configurations and Elastic Constants for Molecular Overlayers on HOPG

	matrix elements[a]								elastic constants (kcal mol^{-1} Å^{-2})[b]						
overlayer	θ	m_{11}	m_{12}	m_{21}	m_{22}	supercell size	*x*[c]	*y*[d]	c_{xx}^{intra}	c_{yy}^{intra}	c_{zz}^{inter}	$c_{a_1a_1}^{inter}$	$c_{a_2a_2}^{inter}$	$c_{a_1z}^{inter}$	$c_{a_2z}^{inter}$
α-$(ET)_2I_3$ (001)[e]	5.8	3.56	0.44	−3.0	5.0	$9\mathbf{b_1} \times 1\mathbf{b_2}$	[100]	[010]	185	108	72	0.5	0.9	0.4	1.2
β-$(ET)_2I_3$ (001)	19.8	2.0	1.0	−4.0	3.3	$1\mathbf{b_1} \times 3\mathbf{b_2}$	[100]	[010]	80	36	44	0.5	0.2	1.0	0.6
β-$(ET)_2I_3$ (011)[f]	17	2.3	1.0	−5.2	8.0	$3\mathbf{b_1} \times 5\mathbf{b_2}$	[100]	[01$\bar{1}$]	36	5	156	1.7	0.9	3.2	1.2
β-$(ET)_2I_3$ ($\bar{1}$10)[f]	17	2.3	1.0	−5.2	8.0	$3\mathbf{b_1} \times 5\mathbf{b_2}$	[001]	[110]	20	40	137	3.0	2.4	2.4	2.5
$(ET)_2ReO_4$ (001)	33.2	1.66	2.0	−5.25	5.0	$3\mathbf{b_1} \times 4\mathbf{b_2}$	[100]	[010]	28	12	51	1.0	1.9	3.0	2.3
$(ET)_2ReO_4$ (011)[g]	36	1.33	2.0	−9.0	6.0	$3\mathbf{b_1} \times 1\mathbf{b_2}$	[100]	[01$\bar{1}$]	15	6	95	2.7	3.2	5.5	7.5

[a] The matrix elements define the azimuthal orientation of the overlayer with respect to the substrate according to

$$\begin{bmatrix}\mathbf{b_1}\\ \mathbf{b_2}\end{bmatrix} = \begin{bmatrix}m_{11} & m_{12}\\ m_{21} & m_{22}\end{bmatrix}\begin{bmatrix}\mathbf{a_1}\\ \mathbf{a_2}\end{bmatrix}$$

as determined with EpiCalc. [b] The elastic constants were calculated from the second derivative at the minimum of the energy versus the respective scalar using a single overlayer unit cell as the basis. [c] The direction along which c_{xx}^{intra} was calculated for each overlayer. [d] The direction along which c_{yy}^{intra} was calculated for each overlayer. [e] The value of θ, the matrix elements and the supercell size correspond to a coincident overlayer found by EpiCalc with lattice parameters suggesting a slightly reconstructed α-$(ET)_2I_3$ (001) layer: $b_1 = 9.35$ Å, $b_2 = 10.74$ Å, $\beta = 90.85°$. These lattice parameters are within 2% of the bulk crystallographic values. [f] The value of θ, the matrix elements and the supercell size were determined with EpiCalc using the mean lattice parameters determined by AFM: $b_1 = 7.2$ Å, $b_2 = 17.3$ Å, $\beta = 83°$. These lattice parameters are consistent with reconstructed β-$(ET)_2I_3$ (011) or ($\bar{1}$10) layers. [g] The value of θ, the matrix elements and the supercell size were determined with EpiCalc using the mean lattice parameters determined by AFM: $b_1 = 7.1$ Å, $b_2 = 19.8$ Å, $\beta = 103°$. These lattice parameters are consistent with a reconstructed $(ET)_2ReO_4$ (011) layer.

AFM data argue that the type II β-$(ET)_2I_3$ overlayer is a slightly reconstructed form of the bulk crystallographic ($\bar{1}$10) layer. This reconstruction is expected to be more facile than for the (001) layer owing to the loss of one of the strong intermolecular interactions (S···S interactions), as is evident from the substantially smaller elastic constants, particularly c_{yy}^{intra}, of the ($\bar{1}$10) overlayer. This energetically unfavorable reconstruction is compensated by the energetic benefit of achieving coincidence. However, the large supercell size of the ($\bar{1}$10) overlayer leads to accumulation of stress from a larger number of noncommensurate overlayer sites than for the (001) overlayer, making the ($\bar{1}$10) overlayer less favorable and accounting for its less frequent occurrence. Similarly, the absence of an α-$(ET)_2I_3$ (001) overlayer can be attributed to the reconstruction and the large supercell required for coincidence. The large intralayer elastic constants for this overlayer make such a reconstruction unlikely.

The influence of supercell size can be surmised further from the observation of the (011) $(ET)_2ReO_4$ overlayer and the complete absence of the (001) orientation. Although the (001) overlayer can achieve coincidence without any perturbation of its native crystallographic form, and thereby preserve both π−π and S···S interactions within the overlayer, the $3\mathbf{b_1} \times 4\mathbf{b_2}$ supercell size results in a substantial number of noncommensurate positions within the supercell. Although the interfacial elastic constants are small for the (001) overlayer, the resulting accumulation of interfacial stress will be larger than that from the smaller $3\mathbf{b_1} \times 1\mathbf{b_2}$ supercell for the coincident (011) overlayer. This is evident from a comparison of the total energies calculated for each of these supercells on HOPG. Calculation of the overlayer−substrate energies indicate that the interfacial energy of the smaller $3\mathbf{b_1} \times 1\mathbf{b_2}$ supercell of the reconstructed (011) overlayer on HOPG is lower (−214.2 kcal mol^{-1}) than that of the $3\mathbf{b_1} \times 4\mathbf{b_2}$ supercell of the bulk (001) layer (−162.7 kcal mol^{-1}). The energy advantage of 51.5 kcal mol^{-1} for the (011) overlayer is associated with fewer noncommensurate overlayer positions in the reconstructed (011) overlayer. This is offset

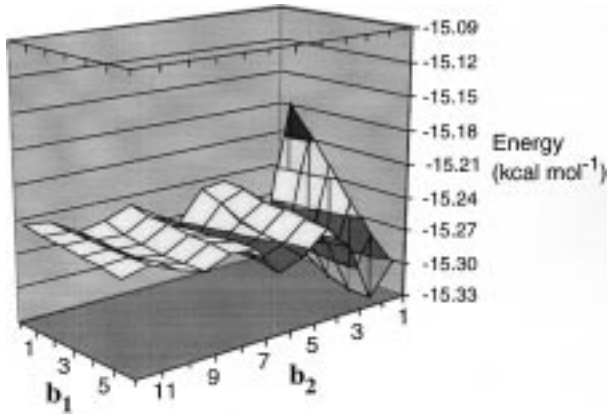

Figure 11. Surface plot depicting the dependence of the overlayer-substrate interaction potential on overlayer dimensions for the β-$(ET)_2I_3$ (001) overlayer. The overlayer dimensions are described in terms of multiples of the primitive unit cell vectors $\mathbf{b_1}$ and $\mathbf{b_2}$. The overlayer−substrate energies were calculated for overlayer sizes corresponding to integral numbers of primitive cells along both vectors, that is, for overlayers with dimensions $Mb_1 \times Nb_2$ with $M \leq 6$, $N \leq 12$. The energy value for each overlayer size was normalized to the number of interactions in one unit cell. Minima along $\mathbf{b_2}$ are separated at intervals of $3b_2$, corresponding to the supercell dimensions along this vector, whereas the potential surface along $\mathbf{b_1}$ is flat owing to the unit repeat of the supercell. The energy minima do not occur at identical energy values because of normalization.

by an energy penalty of 43.7 kcal mol^{-1} for reconstruction, obtained from the difference in the intralayer energies of the reconstructed and unreconstructed (011) overlayer, leaving an energetic benefit of approximately 8 kcal mol^{-1} for the reconstructed (011) layer. It should be noted that the accuracy of these semiempirical calculations may be questionable, particularly because overlayer−solvent interactions have been ignored. Nevertheless, they argue that the overlayer−substrate configuration reflects a delicate balance between the cumulative interfacial stresses resulting from noncommensurate overlayer positions and the perturbation of the overlayer structure from its minimum-energy structure. The (011) orientation is favored by a smaller supercell that contains fewer noncommensurate positions than the rather large supercell of the (001) orientation, even though one of the strong intralayer interactions is sacrificed in the (011) configuration.

The contributions from the commensurate and noncommensurate overlayer sites should result in periodic energy minima at intervals corresponding to the supercell dimensions along the two overlayer lattice vectors. This is evident in surface plots which describe the dependence of the overlayer−substrate interaction energy on overlayer dimensions. For example, minima in the overlayer−substrate energy occur at intervals of $3b_2$ and $3b_1$ for the β-$(ET)_2I_3$ (001) and $(ET)_2ReO_4$ (011) overlayers, respectively, on HOPG (Figure 11). The growth of the 2-D overlayers can be described as a nucleation process in which random assembly events at the HOPG interface eventually produce a nucleus exceeding critical dimensions that is stable and from which growth can occur. The critical size will depend upon the volume free energy of the 2-D nucleus, the overlayer−substrate interactions, and the solvent interactions with the overlayer surfaces, including the molecularly thick step planes exposed at the edges of the overlayer. Estimation of the critical size using semiempirical calculations would require rather tenuous assumptions about the anisotropy of the nuclei and overlayer−solvent interaction energies. Nevertheless, it is reasonable to suggest that the critical nuclei will have dimensions corresponding to the supercell or one of its multiples where the contribution from overlayer−substrate interactions would be optimized.

Conclusions

The observations described here demonstrate that the organization of crystalline molecular overlayers on highly ordered substrates can be governed by coincident epitaxy between the overlayer and substrate rather than by individual molecule−substrate interactions. The assembly of these overlayers and their epitaxial relationship with the substrate can be characterized in real time and in situ by atomic force microscopy, providing considerable insight into the fundamental principles that govern the formation of molecular films. Coincidence is favored for overlayers with at least one strong intralayer interaction that is capable of preventing reconstruction to a purely commensurate lattice and the availability of a coincident match between the overlayer and the substrate. Coincidence permits registry between the substrate and the vertexes of nonprimitive overlayer supercells, thereby lowering the free energy for overlayer formation. However, the presence of a $(ET)_2ReO_4$ (011) instead of a (001) orientation illustrates that the formation of coincident overlayers depends upon supercell size, reflecting a delicate balance of overlayer−substrate and intralayer energetics. The less frequent appearance of the β-$(ET)_2I_3$ ($\bar{1}10$) overlayer can be attributed to its large supercell, the presence of only one strong intralayer interaction, and the energetic penalty associated with a slight reconstruction from its native structure. These results demonstrate that the design of molecular overlayers and prediction of their structure based on layered motifs in 3-D crystal structures should include layers other than ones with the strongest 2-D interactions. Nevertheless, design strategies based on crystallographic layers and analysis of the mode of epitaxy and degree of overlayer−substrate match provide a "crystal engineering" approach to the fabrication of molecular thin films. Furthermore, such studies provide insight into the selectivity observed for polymorphs of bulk crystals grown on electrode substrates such as HOPG. Further studies such as those described here, particularly those involving films in which growth is controlled electrochemically, will contribute substantially to the understanding of nucleation and growth of organic thin films and crystals. We anticipate that this understanding can lead to unique opportunities in nanoscale processing of functional thin films in which the properties of the films can be adjusted rationally by changes in the molecular structure of the components.

Acknowledgment. The support of the Office of Naval Research and the Center for Interfacial Engineering (NSF Engineering Research Centers Program) are gratefully acknowledged. J.A.L. also acknowledges the support of a University of Minnesota Doctoral Dissertation Fellowship.

CM970582S